Energy 348 (2026) 140542

Contents lists available at ScienceDirect

Energy

journal homepage: www.elsevier.com/locate/energy

Numerical and experimental analysis of a new direct-contact PVT system for sustainable energy production: Energy, exergy, and environmental assessments

Yassine El Alami [a,*], Hicham El Achouby [a], Rehena Nasrin [b], Charaf Hajjaj [a], Mohammadi Benhmida [a], Elhadi Baghaz [a], Mohammed Ghazal [c], Adnan Ibrahim [d,**]

[a] Laboratory of Electronics, Instrumentation and Energetic, Faculty of Sciences, Chouaïb Doukkali University, El Jadida, Morocco
[b] Department of Mathematics, Bangladesh University of Engineering and Technology, Dhaka, 1000, Bangladesh
[c] Electrical, Computer and Biomedical Engineering Department, Abu Dhabi University, Abu Dhabi, PO Box 59911, United Arab Emirates
[d] Solar Energy Research Institute, Universiti Kebangsaan Malaysia, Bangi, Selangor, 43600, Malaysia

ARTICLE INFO

Keywords:
Direct fluid-panel contact
Energy-exergy performance
Numerical-experimental understanding
PVT system
Sustainability

ABSTRACT

This study proposes a new photovoltaic-thermal system (PVT-S) in which water is directly connected to the rear of the photovoltaic (PV) module, eliminating the traditional absorber plate in order to improve thermal management, reduce pressure losses, and lighten the system's structure. This configuration addresses the issues of temperature inhomogeneity, thermal expansion, and excessive weight observed in conventional PVT-Ss, highlighting its importance in improving the performance and durability of hybrid solar systems. The proposed configuration was studied numerically using the finite element method in COMSOL Multiphysics, then validated experimentally under real environmental conditions in El Jadida for different mass flow rates, analyzing temperature distribution, pressure losses, energy and exergy performance, as well as several sustainability indicators such as waste exergy ratio (WER), sustainability index (SI), ecological efficiency index (EcEI), and improvement potential (IP), in addition to exergy destruction and entropy generation. The results indicate that this configuration demonstrates improved temperature distribution and lower pressure loss (18.16 Pa) at a high flow rate of 0.0500 kg/s. Furthermore, at a flow rate of 0.0417 kg/s, the maximum temperature difference, power output, and electrical efficiency between the PVT-S and the reference PV panel are 25.38 °C, 19.03 W, and 1.46%, respectively. The mean energy-exergy efficiencies of the PVT-S reach 75.83% and 17.56%, respectively. The peak values for SI, WER, IP, and EcEI are 1.21311, 0.85402, 1089.47 W, and −0.64865, respectively. These results suggest that the proposed configuration is an effective solution for simultaneously improving the energy performance, exergy quality, and overall sustainability of PVT-Ss.

Nomenclature

Abbreviations			
EcEI	Ecological efficiency index	A_{PV}	PV area (m^2)
EVA	Ethylene vinyl acetate	T_{out}	Output water temperature (°C)
PVT-S	Photovoltaic thermal system	u, v, w	Velocity components (m/s)
WER	waste exergy ratio	$\dot{X}_{des}$	Exergy destruction
EEF	Electrical efficiency	$\dot{X}_{el}$	Electrical exergy (W)
FF	Form factor	V_{oc}	Open-circuit voltage

(continued on next column)

(*continued*)

Abbreviations			
MFRT ($\dot{m}_f$)	Mass Flow rate	C_p	Specific heat (J Kg^{-1} K^{-1})
SI	Sustainability index	$T_{in,f}$	Inlet temperature (°C)
FEM	Finite element method	v_{in}	Input velocity (m/s)
IP	Improvement potential	$\dot{X}_{sun}$	Exergy solar radiation
TEF	Thermal efficiency	n	Surface normal
PVT-Ss	Photovoltaic thermal systems	$\dot{E}_{el}$	Electrical power (W)
Parameters		$\dot{E}_{el}$	T_c

(continued on next page)

* Corresponding author.
** Corresponding author.
E-mail addresses: yassineelalami97@gmail.com (Y. El Alami), iadnan@ukm.edu.my (A. Ibrahim).

https://doi.org/10.1016/j.energy.2026.140542
Received 17 December 2025; Received in revised form 12 February 2026; Accepted 21 February 2026
Available online 22 February 2026

(*continued*)

Abbreviations			
K	Thermal conductivity (W m^{-1} K^{-1})	I_{sc}	Short-circuit current
T_{ted}	Tedlar temperature (°C)	$T_{out,f}$	Outlet temperature (°C)
$\dot{E}_{sun,in}$	Received energy (W)		
P_c	Packing factor (%)	**Greek Symbols**	
$\dot{S}_{gen}$	Entropy generation	ε_{PVT}	Exergy efficiency (total) (%)
$\dot{E}_{th}$	Thermal energy (W)	ε_{el}	Exergy efficiency (electrical) (%)
Ts	Surface temperature, (°C)	ε_{th}	Exergy efficiency (thermal) (%)
T_g	Glass temperature (°C)	ρ	Density (Kg m^{-3})
$\dot{X}_{th}$	Thermal exergy (W)	η_{th}	Thermal efficiency (%)
Q	Heat flow vector	η_{el}	Electrical efficiency (%)

1. Introduction

The widespread use of fossil fuels is a major cause of environmental damage because they release pollutants and greenhouse gases that make global warming worse. This reliance on fossil fuels meets a large part of the world's energy needs [1], which shows how important it is to switch to renewable energy sources [2]. This background has led to more people wanting to make renewable and sustainable energy solutions [3]. Among the different energy sources accessible, solar energy stands out due to its abundance, renewable nature, and capacity to provide clean electricity [4]. Large-scale deployment of PV systems is appealing due to their capacity to directly convert sunshine into power, their low environmental impact, and their steadily declining costs [5]. However, the effectiveness of solar panels is severely limited by operational temperature. Efficiency may drop by as much as 0.45 to 0.5% per °C for every degree Celsius that the temperature rises over the usual test settings of 25 °C [6]. Panels in high-temperature regions can achieve temperatures of more than 85 °C, which has an impact on energy production as well as the durability of the silicon, encapsulants, and connectors utilized in the modules [7]. Rise in temperature speeds up the wear of components and compromises long term reliability of solar systems by enhancing internal resistance and recombination losses [8]. In order to address this limitation, PVT-S systems are able to recover as much as possible of solar energy through incorporating both heat recovery and electricity generation [9]. These gadgets may efficiently supply low-temperature heat and electrical energy at the same time, satisfying both residential and commercial needs [10]. In comparison to a conventional PV module of comparable size, research has demonstrated that a well-designed PVT-S can double the total energy generated while meeting the hot water needs of a typical household [11]. PVT-Ss are great for situations where you need a reliable and cheap source of heat and electricity because they can

Table 1
Summary of geometric designs of thermal exchangers.

References	Years	Type of study	Absorber configuration	Major outcomes
[22]	2023	Experimental	Spiral and serpentine thermal collector	Maximum EEF increases by 0.53% with a 5.6 °C drop in module temperature. Insulation enhances TEF by up to 18.26%, but slightly reduces EEF, highlighting the need to balance both performance aspects in system design.
[23]	2019	Experimental	Parallel serpentine tube	PVT-S achieved a maximum exergy efficiency of 12.98% at 0.5 LPM, an EEF of 10.46% (compared to 9.89% for PV alone), and a maximum TEF of 76.58% at 2 LPM.
[24]	2021	Numerical	Periodically grooved channels	The grooves lower the PV's average temperature by 4 K and improve heat transfer via vortices. Rectangular grooves cause the greatest pressure drop, while longer grooves increase convection but also increase flow resistance, and groove spacing has a minimal effect on overall performance.
[5]	2025	Numerical	New serpentine tube	Panel temperature reduction of 5.5 K, EEF improvement of 2.48%, thermal fluctuations limited to 4 K, and PCM melting time extended by up to +142% depending on water flow rate.
[25],	2021	Experimental and numerical	Serpentine tube	PVT-S with serpentine tube configuration increases the total system efficiency to 51.76%, achieves a thermal and EEF of 48.4% and 7.3%, respectively, demonstrating a significant improvement over the no-cooling scenario.
[26]	2023	Numerical	Roll Bond collector	Uneven flow distribution in the microchannels causes areas of higher temperatures and a drop in electrical output. EEF is enhanced by 10.3–14.5% compared to PV alone for inlet water temperatures ranging from 20 to 30 °C.
[27]	2025	Experimental	Flat heat sinks with serpentine tubes and paraffin wax	Nanofluids, especially those based on graphene, lower cell temperatures and increase power as well as electrical and thermal efficiencies, with better performance at higher concentrations and flow rates.
[28]	2020	Experimental and numerical	Roll-bond heat exchanger with three channel geometries: series, parallel, and bionic	The bionic absorber offers the best overall performance, characterized by lower water outlet temperatures, reduced pressure losses, and maximum electrical and exergy efficiencies (9.9% and 12.7%). PVT-S remains less thermally efficient (33.5%) compared to the solar thermal module (61.4%).
[29]	2025	Numerical	channel structure integrated with perforated V-shape fins	Cell temperature reduction of approximately 31% and EEF improvement of approximately 19%, superior to straight fins (≈20%) and channel boxes (≈18%).
[30]	2025	Numerical	Serpentine tube absorber with fins	The fins reduce the temperature of the cells by approximately 3 K and improve EEF by 0.65 to 1.38% depending on the flow rate, while increasing the liquid fraction of the PCM by approximately 10% and the stored energy by approximately 51.7 kJ. The Ag-rGO nanofluid offers the highest thermoelectric performance.
[31]	2024	Experimental and numerical	branch-inspired channel in roll-bond type	The best RB configuration achieved an EEF of 17.75% and a TEF of 61.86%, resulting in an overall efficiency of 79.56%, which represents a 20.4% increase in EEF compared to the reference system.
[32]	2024	Experimental	Semicircular absorber tubes	PVT-S using nanofluid system and NPCM have a TEF of 78.99% and an EEF of 12.70 %, and the surface temperature of PVs reduces by a factor of about 35 %, which is highly beneficial to the overall performance of the device.
[33]	2024	Numerical	Three equal zigzag-plated tube sections	The new arrangement is more efficient in terms of TEF by 7.23 %, 15.75%, and EEF by 4.0%, 4.6%, respectively to the systems of water and air. The change is to provide even cooling and minimizes temperature variations throughout the panel.
[34]	2023	Numerical	Collector integrated with flax fibers as natural porous materials	The maximum TEF reaches 69.58%, and the Nusselt number increases from 18.65 to 51, representing a 173% improvement over water alone.
[35]	2023	Experimental	Split flow and Parallel-flow	The split-flow collector provides superior thermal performance and efficiency by allowing cold water to arrive on both sides, unlike direct and parallel collectors.

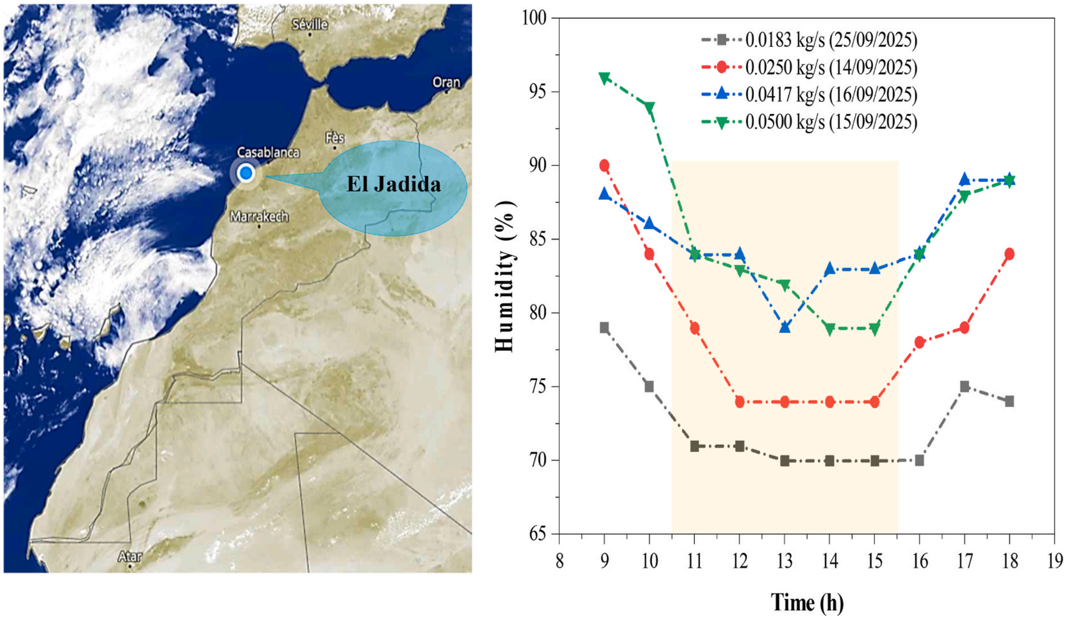

Fig. 1. Geographic location (a) and relative humidity trends (b) during the measurement days in the city of El Jadida.

do both [12]. So, developing and improving PVT-S is a good way to increase overall energy efficiency, extend the life of PV modules, and meet the growing needs of a sustainable energy transition.

It is very important to set up the heat exchanger correctly in order to get the best performance from PVT-S [13]. Since these systems have changed over time, different exchanger configurations have been proposed to make them work better for both electricity and heat. For example, Al-Mamoori and Enes Kilinc [14] considered a new PVT-S that had four new cooling sub-channels. They demonstrated that with 20 × 20 mm^2 sub-channels and a Reynolds number of 2275, they were able to reduce the average temperature of the module to 32.63 °C. In order to accomplish this, they considered the effect of subchannel size and Reynolds number on velocity and thermal profile. This system cools the panels, enhances the thermal performance of the system, and reduces losses due to pressure. Phukaokaew et al. [15] suggested a PVT-S based on magnesium oxide nanoparticles and phase change material (PCM) based on lauric acid. The alteration of the water tube arrangement revealed that the spiral flow with a Reynolds number of 5500 reduced the panel temperature by 3.14 °C, making it an overall efficiency of 80.63 %. One should note that the U-shape design is the most efficient in terms of electricity. Maseer et al. [16] came up with a PVT-S system that included a PCM and a semi-circular tube absorber. The PVT-PCM system had an electrical efficiency (EEF) of 12.23% and thermal efficiency (TEF) of 68.38 %, which was better than that of the PVT-S system without PCM (12.16% and 50.97%). The use of PCM enabled thermal control of the panel and heat removal, which optimized heat loss, minimized overheating, and maximized the production of energy. Azeez et al. [1] studied a new type of PVT-S system, which is a combination of a honeycomb collector in the shape of a petal, a nanofluid, and a phase change material. This design led to a 34 % and 28% efficiency improvement in electricity and thermal efficiency, respectively, over a conventional PVT-S, and the total energy generation was over 27%, and the energy payback time was also shortened by 21%. Zhang et al. [17] suggested a PVT-S where a multi-level V-shaped exchanger is utilized. This design achieved electric efficiency of 9-12% and overall efficiency of more than 65 %. An ideal turbulator solution will allow the enhancement of the heat transfer, as well as panel cooling. In a study by Satpute et al. [18], the spiral absorbers (circular and rectangular) were used in PVT-S with the circulation of water. The rectangular spiral absorber showed a better performance, with the highest electrical performance of 14.32% and a heat recovery rate of 63.56%. Zhang et al. [19] investigated a direct expansion PVT-S with a T-shaped evaporator exchanger. Their structure reduced the panel temperature by 8.5 to 13 °C than traditional panels and honeycomb PVT-Ss, which led to an increase in instant electrical power as much as 56.6% with a rise in overall output of 9.3 to 14.5 %. The photoelectric efficiency was 21.5% to 22.6%, and the system allows saving up to 386.50 yuan annually. Sheikholeslami et Khalili [20] studied a PVT-S using an 8-lobe section tube heat exchanger instead of a circular tube, with internal copper fins and GNP nanofluid. This configuration enhanced heat transfer, resulting in an approximately 5.8% increase in electrical performance and achieving a TEF of approximately 55%, with a payback period of less than 2 years. Hosouli et al. [21] studied a PVT-S incorporating an aluminum alloy absorber with an H-shaped expansion cavity heat exchanger placed between the PV cells and the absorber to reduce thermal expansion and thus the risk of cell cracking. The results show that the optimal configuration (2 mm cavities) reduces thermal deformation by 20% and improves thermal, electrical, and overall performance by 10%, 2%, and 8%, respectively, compared to the reference collector. Table 1 summarizes other studies that have examined different geometric designs of heat exchangers in PVT-Ss.

Several configurations have been designed and tested to improve their overall performance. Even recent developments have not solved the thermal management issues in PVT-S systems. Existing analyses indicate growing interest in these systems and their opportunities, as well as gaps in knowledge about their thermal dynamics. Further studies are needed to improve the efficiency of PVT technology and fill the following gaps.

- Most of the geometries studied and proposed still use flat heat exchangers (coils, plates, and tubes, etc.). This type of design creates temperature heterogeneity due to the spaces between the tubes, which reduces overall performance and accelerates the aging of PV cells.
- In most research, the absorbing plate is inserted between the PV module and the fluid circulation tubes, which limits heat transfer between the fluid and the panel.
- 2
- There is a notable gap in the literature on heat exchangers that allow direct contact between the back of PV panels and the heat transfer

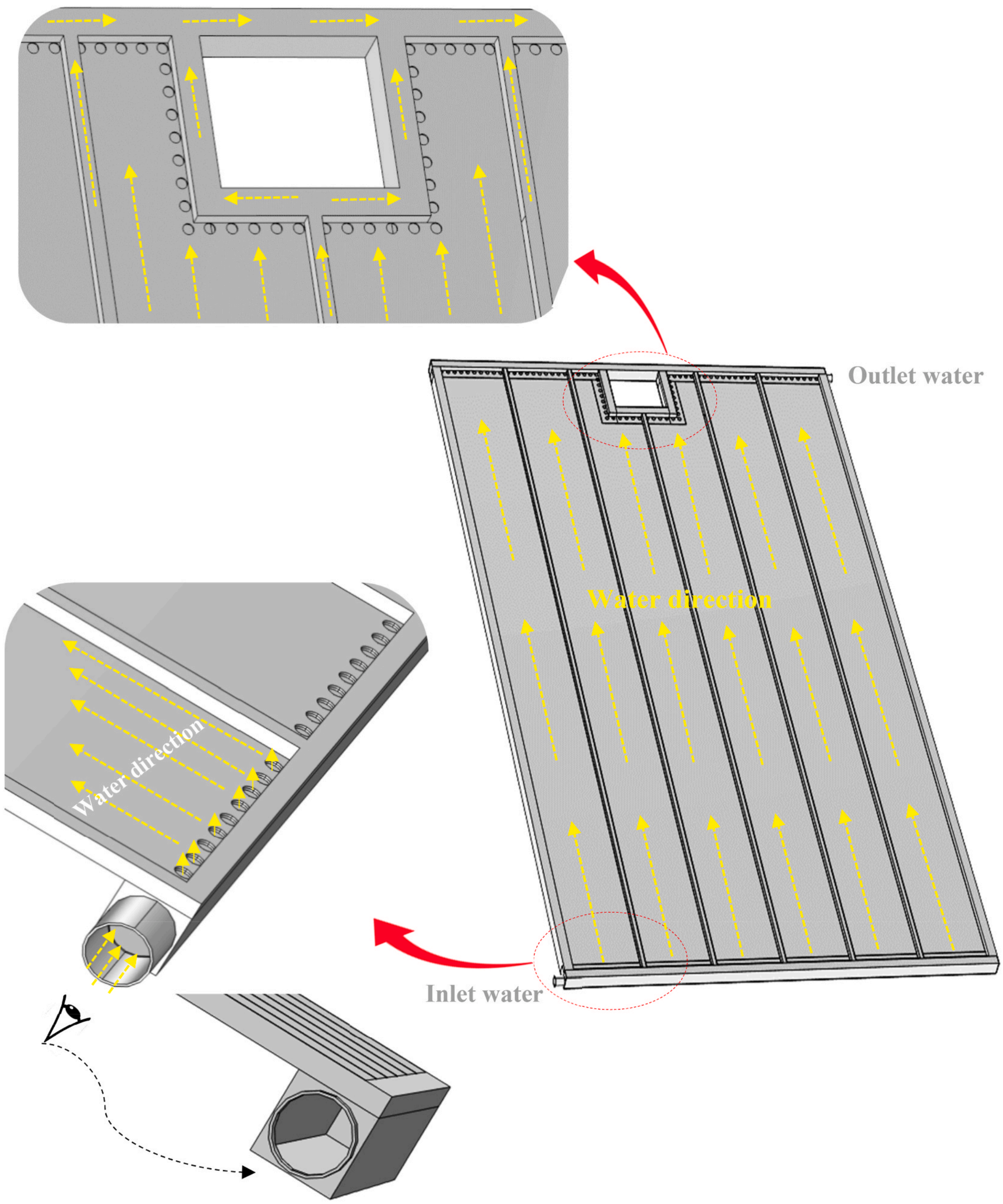

Fig. 2. Overview of the proposed design for the stainless steel heat exchanger.

fluid, which presents an opportunity for innovation to improve the TEF and performance of PV systems.

- Most of the geometries proposed have been studied solely using numerical methods, without experimental confirmation to validate them.
- The PVT-S studied in the literature generally suffers from significant pressure drops, which is a major constraint on its operation.

This study aims to fill the gaps identified in the literature by proposing a new heat exchanger design for PVT-Ss, characterized by direct contact between the heat transfer fluid and the rear surface of the PV module. Unlike conventional configurations based on an intermediate absorber plate, the solution developed reduces the system's weight, limits the stresses associated with thermal expansion, and decreases hydraulic pressure losses, while enhancing heat extraction. The originality of the work also lies in the methodological approach combining three-dimensional numerical modeling using COMSOL Multiphysics and experimental validation carried out under real climatic conditions in El Jadida. The comprehensive evaluation of the system includes detailed analysis of temperature and pressure fields, study of energy and exergy performance at different mass flow rates (MFRTs), and in-depth analysis of sustainability using several advanced indicators such as the sustainability index (SI), waste exergy ratio (WER), improvement potential (IP), ecological efficiency index (EcEI), exergy destruction, and entropy generation.

2. Experimental setup

2.1. Climatic data

El Jadida is a Moroccan coastal city located on the Atlantic coast, in the Casablanca-Settat region (Fig. 1a) [36]. It is situated about 96 km southwest of Casablanca and has an average altitude of 10 m above sea level, at a latitude and longitude of 33°15′ N and 8°30′ W, respectively.

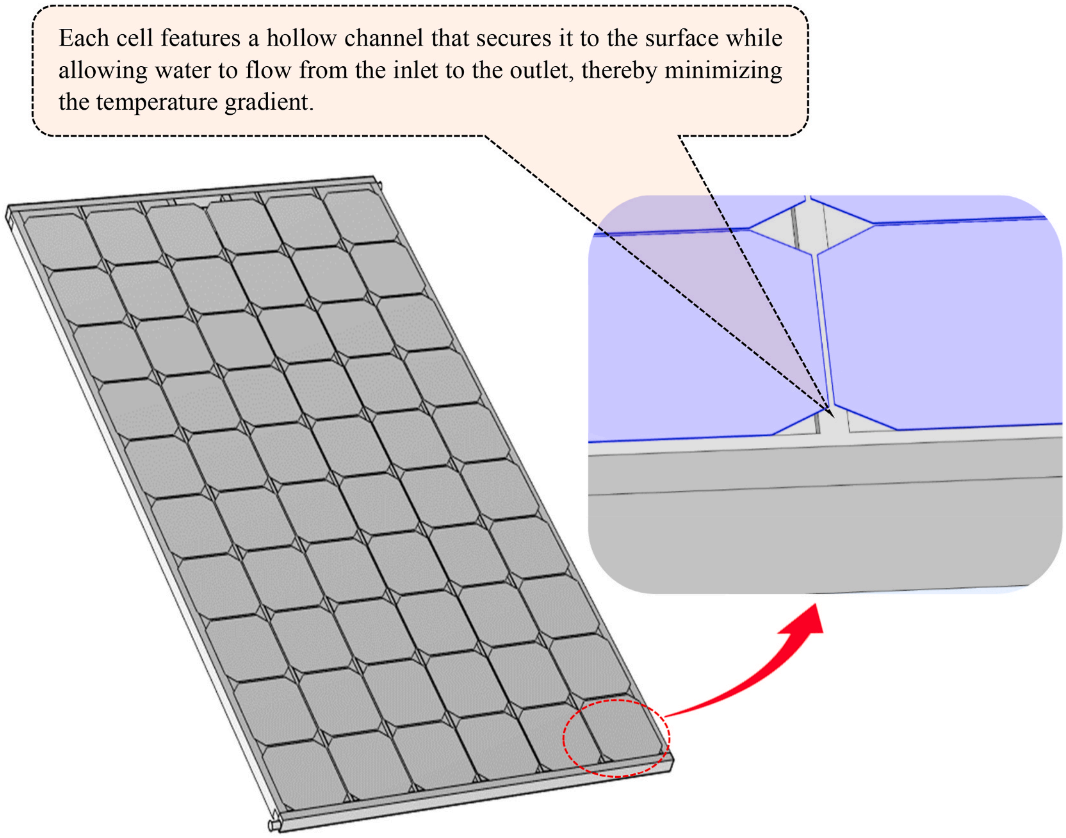

Fig. 3. Image of the hollow channel that was incorporated between the PV cells to allow water circulation.

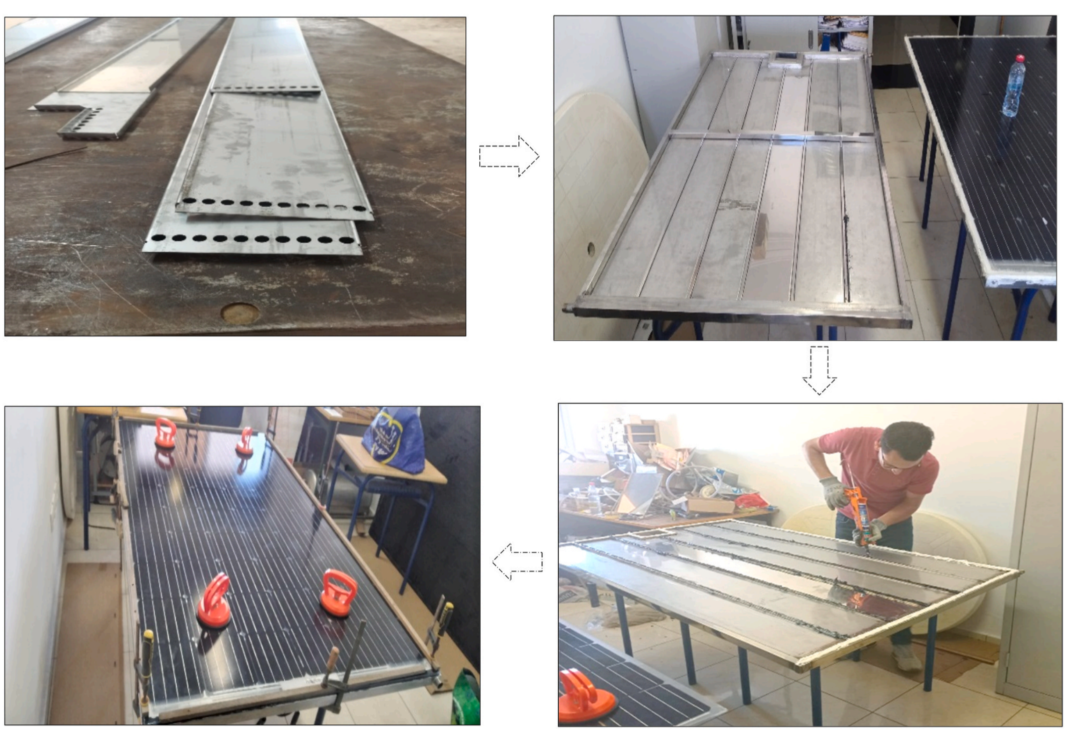

Fig. 4. Experimental process stages for fabrication and assembly of the new design integrated into the PV panel.

Due to its coastal location, El Jadida is characterized by relatively high humidity, especially in the early morning and evening, as illustrated in Fig. 1b. Some of the equipment used in this study, such as the I-V tracer, is sensitive to humidity and should not be used in environments where humidity exceeds 80% [37], in order to avoid any risk of failure. For this reason, the experimental measurements were carried out between

Table 2
Technical specifications of the Almaden SEAC60T-300 PV panel under STC.

Parameters	Symbol	Unit	Value
Conversion efficiency	η_{ref}	%	18.237
Rated (nominal) power	P_{max}	W	300
Maximum power point current	I_{mpp}	A	9.26
Module surface area	A	m^2	1.64538
Short-circuit current	I_{sc}	A	9.73
Temperature coefficient of open-circuit voltage	-	%/°C	−0.3
Maximum power point voltage	V_{mpp}	V	32.40
Temperature coefficient of short-circuit current	-	%/°C	0.06
Open-circuit voltage	V_{oc}	V	39.87
Temperature coefficient of maximum power	-	%/°C	−0.39

10h44 and 15h, when humidity levels are at their lowest.

2.2. Design and fabrication of the PVT system

A new heat exchanger design, constructed from stainless steel, has been proposed to address the limitations identified in the scientific literature. Here, every PV cell's string is connected with a specific 10 mm water blade, as illustrated in Fig. 2. The straight connection of cells-water enhances thermal treatment efficiency. A hollow channel is incorporated between each cell (Fig. 3), effectively securing the cells to their substrate and facilitating the flow of water from the inlet to the outlet. This design reduces the temperature gradient, resulting in a more uniform temperature throughout the system. Fig. 2 also shows that the heat exchanger has two 30 mm high manifolds, which serve to distribute the water across all layers. Each aquifer has its own supply and outlet zones. The fluid first enters the inlet manifold before passing through the aquifers (Fig. 2). This is done in an upward direction, with the water distributed evenly towards the outlet of the system. Thermal paste is used to secure the new design in the PV panel. Fig. 4 shows the different stages of the manufacturing and assembly process. The PV panel used in this work is an Almaden glass-glass monocrystalline model (SEAC60T-300). Table 2 shows the main characteristics of the PV panel under standard test conditions (STC).

2.3. Experimental set-up

The experimental system comprises a PV panel and a PVT-S mounted side by side, and data will be collected simultaneously on both systems (Fig. 5). Drinking water is poured into a 30-L tank to provide the amount of water needed to operate the PVT-S. A variable speed electronic circulation pump (DAB Evotron circulator) ensures continuous fluid circulation in the open circuit. It offers a flow rate range of 0.4 to 4.2 m^3/h, a maximum head of 8 m, and can operate with fluids at temperatures ranging from −10 °C to +110 °C, under a maximum operating pressure of 10 bar (1000 kPa). A flow meter and a manual valve regulate the water flow in this system to ensure perfect control. When water flows through the PVT-S heat exchanger, it absorbs the thermal energy produced by the PV cells. This heat can be used to heat buildings and swimming pools and even to supply domestic hot water, making buildings and swimming pools more energy efficient.

The performance of both PV and PVT-Ss was analyzed in detail during the experiment. The most important parameters that were tracked were the system temperatures, fluid flow rates, and inlet and outlet water temperatures, the solar irradiance, ambient temperature, and electrical parameters of voltage, current, and power output. Temperature distribution on the surfaces of the two systems was also studied in order to gain some insight into the thermal behavior of the two systems. Fig. 6 presents the experimental setup, and the sensors, as well as the instruments, are depicted. The modules had four K-type thermocouple probes that were connected to an Arduino Mega board to record temperatures every 10 min. The temperature of the inlet water was

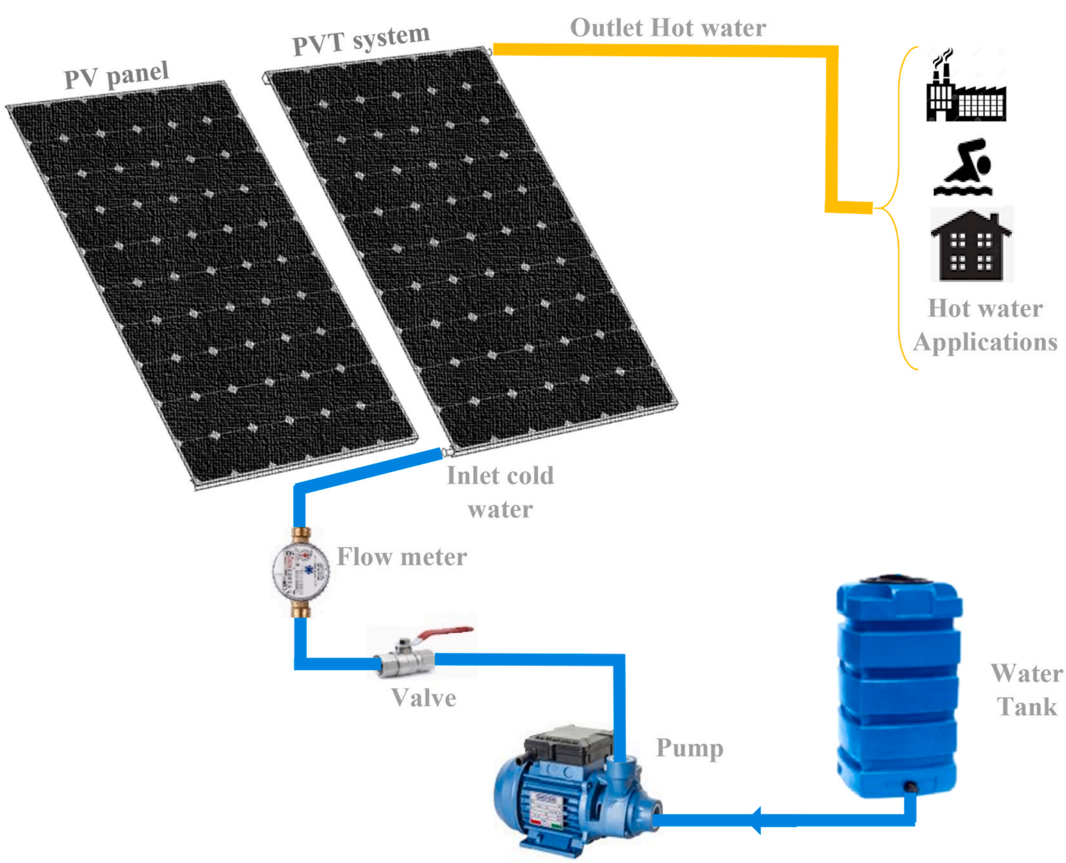

Fig. 5. Water circuit and experimental arrangement.

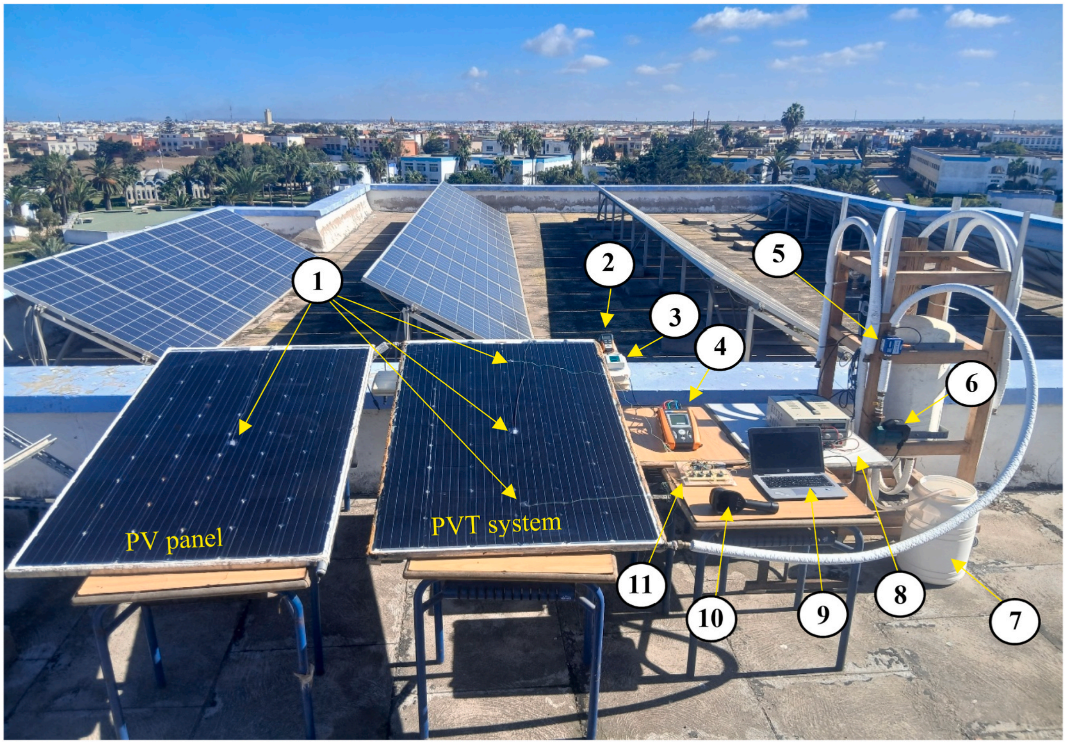

Fig. 6. Experimental setup of PV and PVT-Ss with measuring instruments. Note: (1) Thermocouples, (2) Solar 02, (3) HT304N reference cell, (4) I–V tracer, (5) Flow meter, (6) Pump, (7) Reservoir tank, (8) Mercury thermometer, (9) Computer, (10) Infrared camera, and (11) Data acquisition and transmission system.

Table 3
Technical specifications of measuring instruments.

Equipment and models	Used to measure	Measurement range	Uncertainty
HT I-V400 solar tracer	The voltage, current, and power of PV and PVT-Ss	-	1 %
Mercury thermometer	The inlet temperature of the circulating fluid	0 °C to 100 °C	±0.5 °C
FLIR E5 Pro infrared camera	Temperature distribution on the surface of PV and PVT-Ss	−20 °C to 400 °C	±2%
Thermocouple (type K)	Outlet water temperature and temperature of PV and PVT-Ss	−200 °C to +1350 °C	±2%
HT304N reference cell	The solar irradiance received by the panels	50-1400 W/m^2	±3.0%

monitored using a mercury thermometer that ensured that the temperature was controlled in an accurate manner. An I-V tracer was used to measure electrical parameters that were used to obtain information on current, voltage, and power. A SOLAR-02 gauged the ambient temperature, whereas solar radiation was measured by an HT304N reference cell. The flow rate of the water was measured using a MAG-VIEW MVM-030-PA flow meter, which has a control valve to adjust the flow. The thermal distribution of the modules was observed using an infrared camera, and this could be analyzed to study the heat transfer of the PVT-S system and the PV panel. Table 3 summarizes equipment specifications.

2.4. Uncertainty analysis

The validity of the experimental data was determined by the uncertainty analysis. Instrument tolerances were supplied by the manufacturers, and they are given in Table 3. The results were measured by a 95% confidence interval [22] to determine the reliability of the results. The total uncertainty was computed based on equation (1) [38] and amounts to ±4.24 %, and this is less than the allowed mark of 5% [22], and therefore the results indicate the validity of the measurements.

$$\omega L = \sqrt{\left(\frac{\partial L}{\partial H_1}\omega_1\right)^2 + \left(\frac{\partial L}{\partial H_2}\omega_2\right)^2 + \ldots\ldots + \left(\frac{\partial L}{\partial H_n}\omega_n\right)^2} \quad (1)$$

Where ωL is the efficiency uncertainty, and H_1 to H_n are the dependent variables.

2.5. Mathematical analogy

2.5.1. Energy assessment

The PVT-S can be modeled as a single control volume (Fig. 7), which allows for a clear description of the distribution of absorbed solar energy ($\dot{E}_{in}$). This is divided into electrical energy produced ($\dot{E}_{el}$), heat transferred to the fluid ($\dot{E}_{th}$), and heat losses to the environment ($\dot{E}_{loss}$). Equation (2) displays the steady-state energy conservation [39].

$$\dot{E}_{in} = \dot{E}_{loss} + \dot{E}_{th} + \dot{E}_{el} \quad (2)$$

The solar energy received by the system is given by equation (3), where A_{PV} is the surface area of the PV module, and G is the solar irradiance. The electrical power generated, $\dot{E}el$, is calculated using Equation (4), which utilizes the open-circuit voltage (V_{oc}) and short-circuit current (I_{sc}) of the module [40]. The form factor (FF), representing the maximum conversion efficiency, is determined by equation (5) [27].

$$\dot{E}_{sun} = A_{PV} \cdot G \quad (3)$$

$$\dot{E}_{el} = V_{oc} \cdot I_{sc} \cdot FF \quad (4)$$

$$FF = \frac{P_{max}}{V_{oc} \cdot I_{sc}} = \frac{V_{max} \cdot I_{max}}{V_{oc} \cdot I_{sc}} \quad (5)$$

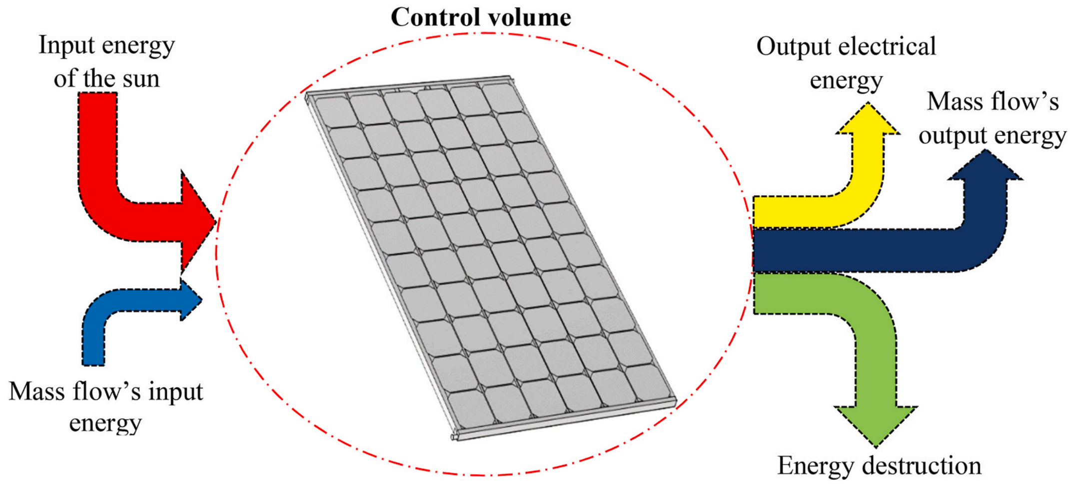

Fig. 7. Diagram of the control volume for the energy assessment of the system.

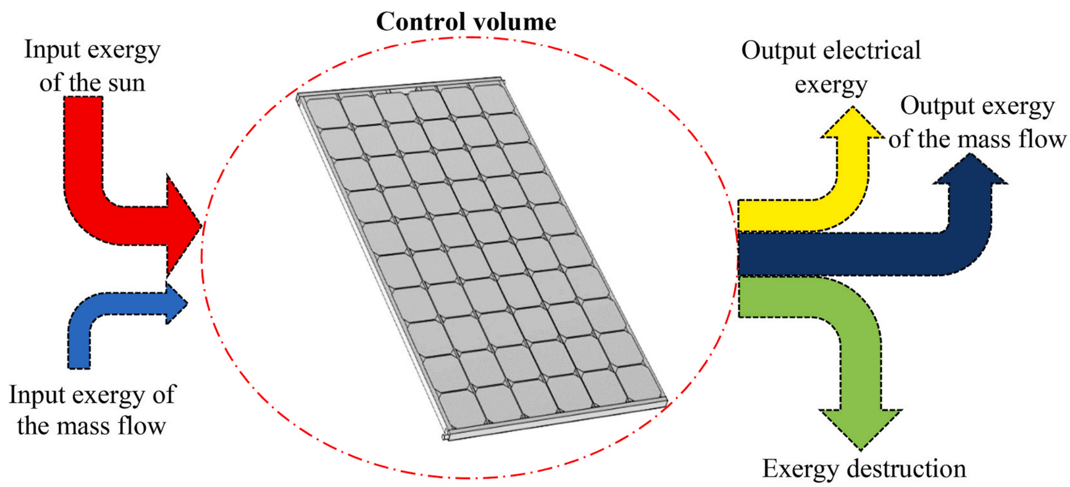

Fig. 8. Diagram of the control volume for exergy evaluation of the system.

Table 4
Geometric dimensions and thermal properties of PVT-S components [46].

Material Layer	Thickness (mm)	C_p (J/kg.K)	ρ (kg/m^3)	k (W/m.K)
Glass	2.5	750	2200	1.8
Stainless steel	-	502.48	8030	16.27
EVA	0.5	2400	935	0.29
Water	-	4181.8	998	0.68
Silicon	0.19	703	2329	148

Table 5
Optical and environmental properties used in the numerical model [47].

Description	Symbol/Unit	Values
Standard reference temperature	T_{ref} (°C)	25
Glass layer emissivity	ε_g	0.04
Glass optical transmittance	τ_g	0.96
Heat transfer coefficient between glass and ambient air	$U_{g\text{-}amb}$ (W/m^2.K)	10
PV module packing factor	P_c	0.95
PV cell absorption coefficient	α_c	0.9

The useful thermal energy produced can be expressed by equation (6), while the electrical, thermal, and overall efficiencies are calculated using equations (7)–(9), respectively [41]:

$$\dot{E}_{th} = \dot{m}_f \cdot c_{p,f} \cdot \left(T_{f,out} - T_{f,in}\right) \tag{6}$$

$$\eta_{el} = \frac{\dot{E}_{el}}{\dot{E}_{sun}} \tag{7}$$

$$\eta_{th} = \frac{\dot{E}_{th}}{\dot{E}_{sun}} \tag{8}$$

$$\eta_{ov} = \frac{\dot{E}_{el} + \dot{E}_{th}}{\dot{E}_{sun}} \tag{9}$$

2.5.2. Exergy assessment

When studying a solar energy conversion system, an assessment based solely on energy does not enable us to distinguish between useable energy and available energy. It is due to this that exergy analysis is applied in determining the capability of the system in transforming the energy it receives into useful work. This method considers some of the degradations which take place in the panel, especially because of thermodynamic irreversibility, generation of entropy, and development of temperature gradient within the panel. The total exergy can be formulated by taking the whole device as a control volume in steady state (Fig. 8) by using equation (10) to calculate the total exergy. In this relationship, $\dot{X}_{sun}$ corresponds to the exergy provided by solar radiation, $\dot{X}_{th}$ denotes the exergy associated with heat recovery, $\dot{X}_{el}$ represents the

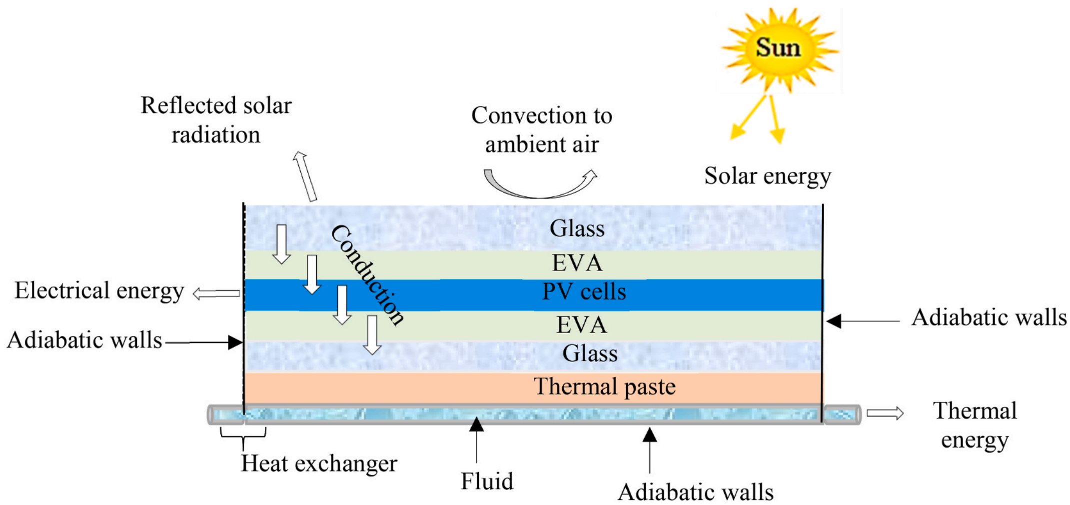

Fig. 9. Overview of the boundary conditions of the PVT-S.

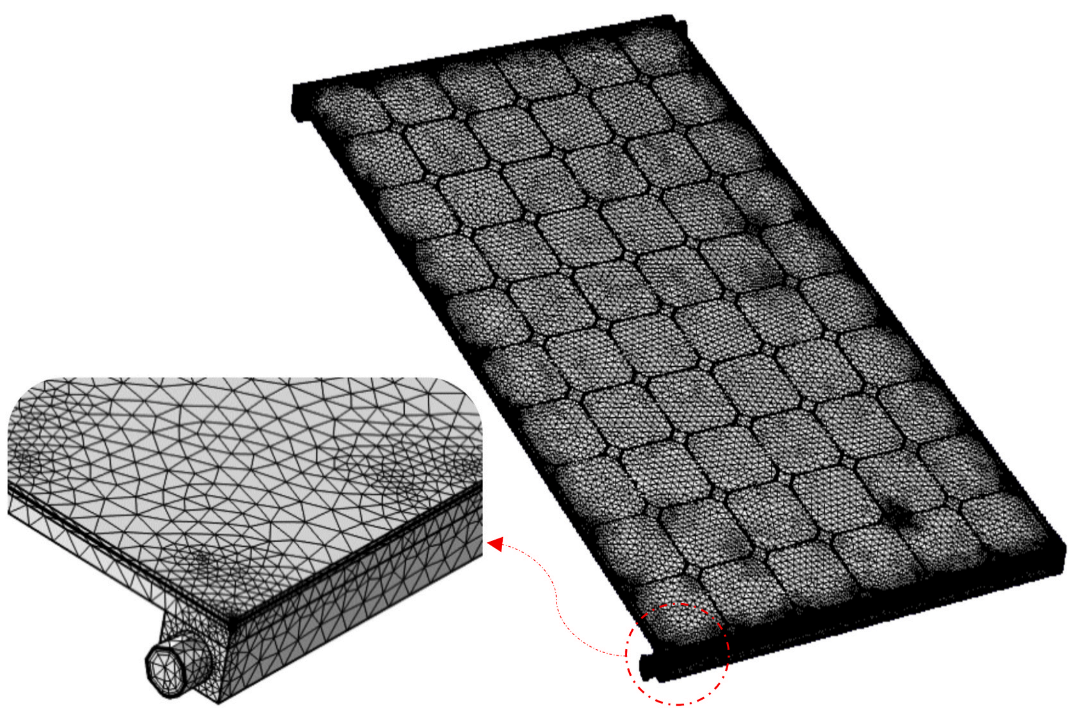

Fig. 10. Detailed view of the mesh applied to the PVT-S.

Table 6
Maximum pressure obtained for different mesh sizes during the mesh independence study.

Mesh type	Number of elements	P_{max} (Pa)	ΔP (Pa)	Calculation time (s)
Coarser	514750	24.87	-	223
Coarse	790096	22.34	2.534	326
Normal	1298558	19.28	3.058	453
Fine	1675550	18.16	1.124	638
Finer	3804079	17.98	0.564	1564

exergy from electrical conversion, and $\dot{X}des$ expresses the exergy destroyed due to internal losses. The incoming solar exergy ($\dot{X}_{sun}$) is obtained by equation (11), where the surface temperature of the Sun, T_{sun}, is generally taken to be 5770 K. Furthermore, the thermal exergy and electrical exergy, denoted respectively by $\dot{X}_{th}$ and $\dot{X}_{el}$, are calculated using equations (12) and (13) [42].

$$\dot{X}_{sun} = \dot{X}_{des} + \dot{X}_{el} + \dot{X}_{th} \tag{10}$$

$$\dot{X}_{sun} = G \cdot A_{PV} \cdot \left[1 - \frac{4}{3}\left(\frac{T_{amb}}{T_{sun}}\right) + \frac{1}{3}\left(\frac{T_{amb}}{T_{sun}}\right)^4\right] \tag{11}$$

$$\dot{X}_{th} = \dot{m}_f \cdot c_{f,p} \cdot \left(1 - \frac{T_{amb}}{T_{f,out}}\right) \cdot (T_{f,out} - T_{f,in}) \tag{12}$$

$$\dot{X}_{el} = \eta_{el} \cdot G \cdot A_{PV} \cdot \left[1 - \frac{4}{3}\left(\frac{T_{amb}}{T_{sun}}\right) + \frac{1}{3}\left(\frac{T_{amb}}{T_{sun}}\right)^4\right] \tag{13}$$

Equations (14)–(16) are applied to obtain the electrical exergy, thermal exergy, and overall exergy efficiency, respectively [42]:

$$\varepsilon_{th} = \frac{\dot{X}_{th}}{\dot{X}_{sun}} \tag{14}$$

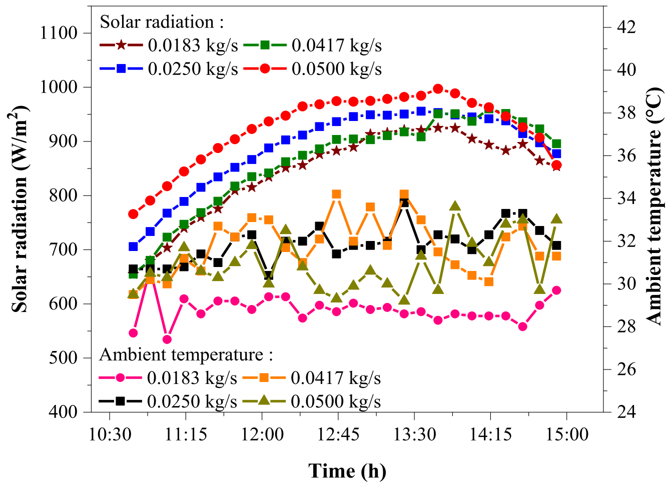

Fig. 11. Daily variation in irradiation and ambient temperature during the four days of PVT-S testing.

$$\varepsilon_{el} = \frac{\dot{X}_{el}}{\dot{X}_{sun}} \tag{15}$$

$$\varepsilon_{PVT} = \varepsilon_{el} + \varepsilon_{th} = \frac{\dot{X}_{out}}{\dot{X}_{sun}} = 1 - \frac{\dot{X}_{loss}}{\dot{X}_{sun}} \tag{16}$$

2.5.3. *Exergy destruction and entropy generation assessment*

The performance of the PVT-S is affected by internal irreversibility, particularly heat loss and friction in the flow channels, which result in exergy destruction. By considering this loss (equation (17)) and the entropy generation (equation (18)) it is possible to measure the loss of available energy and assess the actual efficiency of the system [43]:

$$\dot{X}_{des} = \dot{X}_{sun} - \dot{X}_{el} - \dot{X}_{th} \tag{17}$$

$$\dot{S}_{gen} = \frac{\dot{X}_{des}}{T_{amb}} \tag{18}$$

2.5.4. *Sustainability metrics analysis*

The most important strategies for sustainable development are the optimization of resource use and the use of renewable resources in energy production. The exergy analysis can therefore be considered as a potent tool because it provides an evaluation of how well a system operates under ideal operating conditions. This technique not only determines and minimizes thermodynamic losses but also allows for the development of more efficient systems. Moreover, exergy as a measure of sustainability is a necessary parameter because it is related to the energy and the environmental effects. In this regard, the sustainability index (SI) is used to offer an estimate of the effectiveness of the use of the resources within a given system and is computed based on the exergy efficiency, as presented in the following equation [44]:

$$SI = \frac{1}{1 - \varepsilon_{PVT}} \tag{19}$$

The Waste Exergy Ratio (WER) is the proportion of consumed exergy that is wasted or inefficiently utilized. Low WER indicates the utilization of resources and fewer environmental effects. In this way, the optimization of the WER will have a direct impact on the increase in the sustainability of the system. It is determined with the following equation [45]:

$$WER = \frac{\dot{X}_{des}}{\dot{X}_{in}} \tag{20}$$

The potential for improvement (IP) is used to specify the area within which a system or process can be made more sustainable. It also helps to reveal the possibilities to enhance efficiency, reduce losses, save resources, and mitigate environmental impact with the help of strictly focused interventions. The possible improvement is determined through the equation below [45]:

$$IP = (1 - \varepsilon_{PVT}) \cdot \dot{X}_{des} \tag{21}$$

The Ecological Efficiency Index (EcEI) provides a holistic evaluation of sustainability in the form of a combination of exergy analysis and ecological footprint. It is a quantitative measure of how well a system or process is able to optimize resource use and also reduce the footprint of the system on the environment. High scores of EcEI are associated with the highest ecological performance and more sustainable resource allocation. The calculation of the EcEI will follow the following equation [45]:

$$EcEI = 2 \cdot \varepsilon_{PVT} - 1 \tag{22}$$

3. Numerical investigation

Before implementing the new system, we conducted an in-depth numerical study using COMSOL Multiphysics software, based on the FEM. The 3D simulation, performed in steady state, enabled us to accurately analyze heat transfer and fluid behavior within the PVT-S. The model is based on the actual geometry of the system (see Fig. 4) and incorporates all layers of the monocrystalline silicon PV module. The model includes the top glass, the top EVA layer, the PV cells, the bottom EVA layer, the bottom glass, the stainless-steel heat exchanger, and expanded polystyrene as insulation. In this study, the influence of expanded polystyrene is considered indirectly through the application of boundary conditions. The dimensions and thermal properties of each component are presented in Table 4. The optical and environmental characteristics used in the modeling are listed in Table 5.

3.1. *Governing equations*

Conduction is the only mode of heat transfer in solids in the PVT-S, ensuring the transfer of heat from the PV cells to the fluid [48]:

$$\nabla \cdot (k \nabla T) = 0 \tag{23}$$

Within the fluid channel, heat transfer occurs through a combination of conduction and convection. The equation governing this combined transfer, with water as the fluid, is presented in equation (24) [48]:

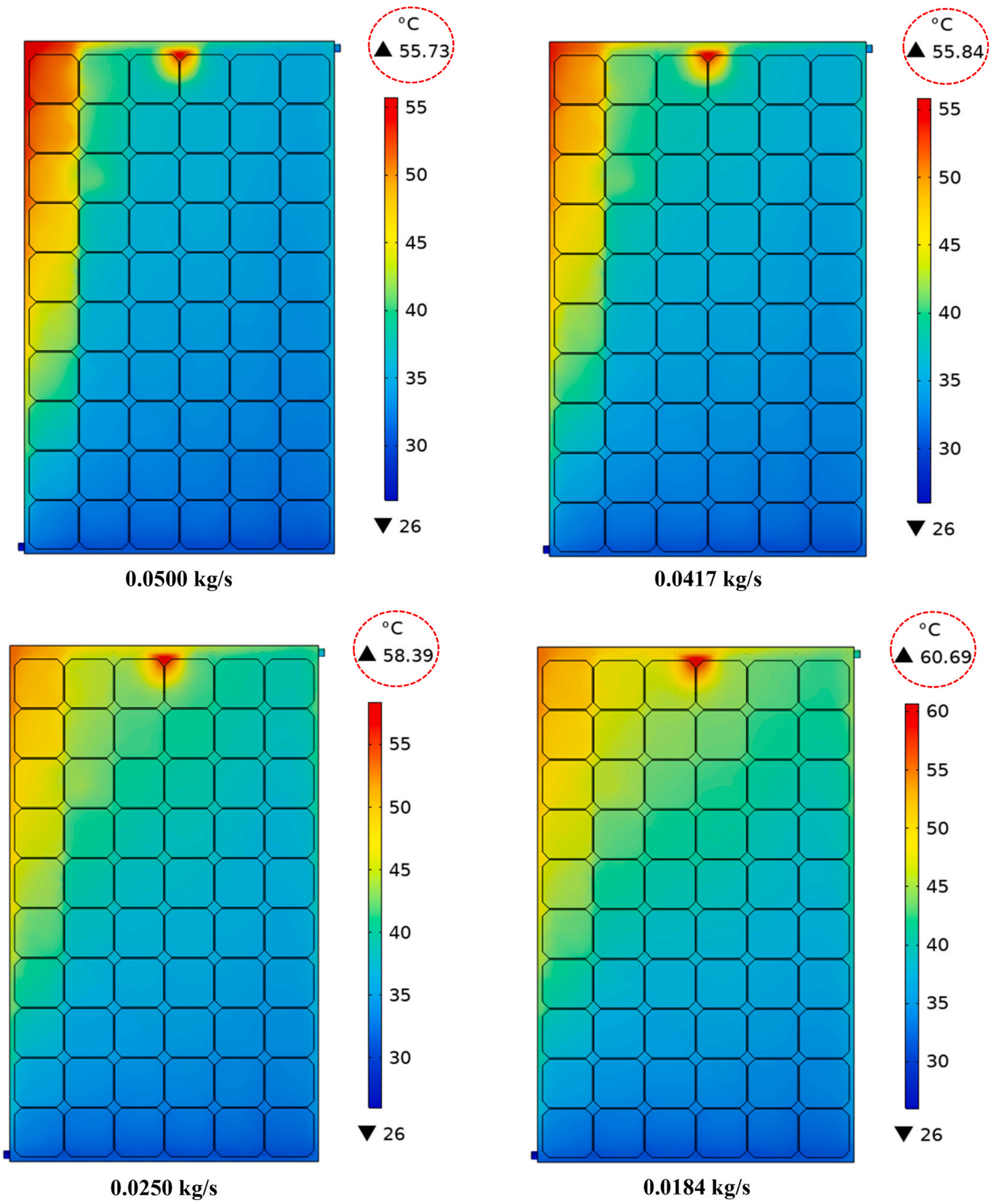

Fig. 12. PV cells' temperature profile obtained by numerical simulation.

$$\rho C_p \frac{\partial T}{\partial t} + \rho C_p u \cdot \nabla T = \nabla \cdot (k \nabla T) + Q \tag{24}$$

The behavior of the fluid is described by the following equations of conservation of mass and momentum [49]:

$$\rho \frac{\partial u}{\partial t} + \nabla \cdot (\rho u) = 0 \tag{25}$$

$$\rho \cdot \frac{\partial u}{\partial t} + \rho (u \cdot \nabla) u = \nabla \cdot \left[-pI + \mu \left(\nabla u + (\nabla u)^T \right] + F \right. \tag{26}$$

3.2. Boundary conditions

Fig. 9 illustrates the boundary conditions applied to the calculation domain, which is defined in accordance with the problem's physics. These include, for the upper layer, an incoming heat flux, convection with the ambient air, and radiation losses, described respectively by equations (27)–(29) [50].

$$-k_g \frac{\partial T_g}{\partial z} = G \tag{27}$$

$$-n \cdot q = h_{g-amb} \cdot (T_{amb} - T_g) \tag{28}$$

$$-n \cdot q = \varepsilon_g \cdot \sigma \cdot ({T_{sky}}^4 - {T_g}^4) \tag{29}$$

where T_{amb}, T_g, and T_{sky} represent the ambient, glass, and sky temperatures, respectively, while n is the surface normal and $h_{g\text{-}amb}$ is the heat transfer coefficient between the glass and the air.

Equation (30) defines the boundary conditions at the inlet to the fluid domain, specifying the flow rate and temperature of the water.

$$T = T_{in}, \dot{m} = \dot{m}_{in} \tag{30}$$

Equations (31) and (32) define the boundary conditions for the wall

(a)
(b)

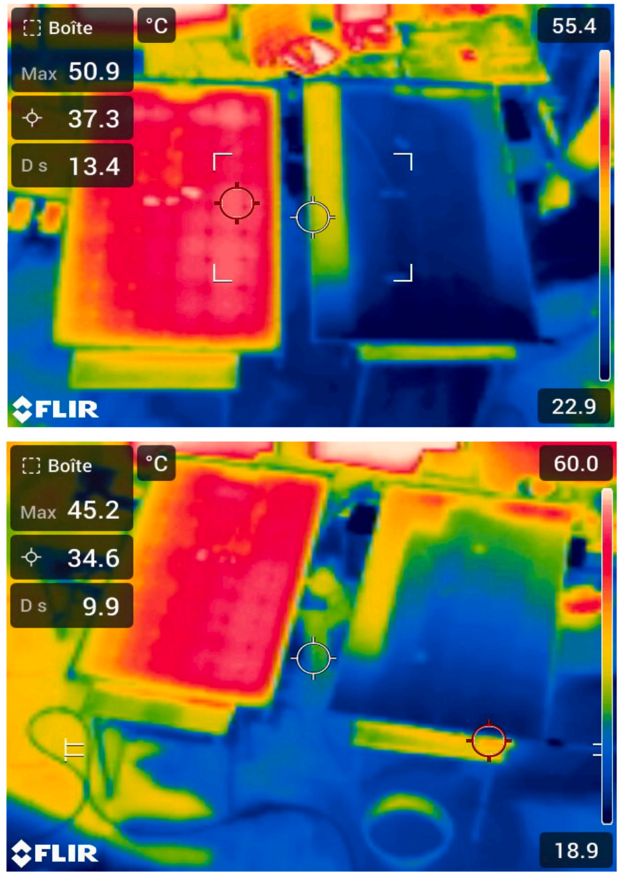

Fig. 13. Experimental thermal images of the PVT-S for MFRT 0.0500 kg/s (a) and 0.0184 kg/s (b).

and the outlet, respectively: the wall is subject to a no-slip condition, while the outlet is set to zero-gauge pressure and no viscous stress.

$$u = 0, v = 0, w = 0 \tag{31}$$

$$P_{out} = 0 \tag{32}$$

The presence of thermal insulation is taken into account in the simulation.

$$-n \cdot (-k \nabla T) = 0 \tag{33}$$

The interface between the water and the absorbent conduit is modeled as a coupled wall, allowing for conjugate heat transfer from the conduit to the fluid.

3.3. *Assumptions*

The COMSOL "Conjugate Heat Transfer" module was used to numerically solve the PVT-S, allowing simultaneous modeling of heat transfer in solids and convection in the fluid. To simplify the model and ensure consistency of results, the following assumptions were made.

- ✓ The underside and edges of the PVT-S are considered to be perfectly insulated [9].
- ✓ The fluid flow is laminar, incompressible, and steady-state [48].
- ✓ The thermophysical properties of materials are assumed to be constant despite temperature variations [51].
- ✓ The effect of dust on solar energy absorption is ignored [52].
- ✓ Ethylene vinyl acetate (EVA) is considered completely transparent to solar radiation [53].

3.4. *Grid independent study*

A mesh independence test was performed to ensure the robustness of the numerical results for the new system under study. The mesh consisted of a combination of free tetrahedral and triangular elements, accompanied by a boundary layer mesh to capture thermal gradients near surfaces (Fig. 10). During the experiment, the irradiance and flow rate were 1000 W/m^2 and 0.05 kg/s, respectively. The pressure (maximum) was evaluated using five different mesh sizes, which ranged from 514,750 to 3,804,079 elements. The results indicated that changes in the number of mesh elements had no significant impact on the maximum pressure observed. As shown in Table 6, the difference between the meshes of 1,675,550 and 3,804,079 elements was negligible. On this basis, a mesh of 1,675,550 elements was selected for the following simulations, ensuring a relative error in maximum pressure of less than 1%.

4. Results and discussion

4.1. *Environment conditions*

During four days of experimentation, environmental parameters were recorded in order to observe the influence of MFRT on the operation of the PVT-S. Each day was associated with a specific flow rate. The system was tested at the following flow rates: 0.0183 kg/s on September 25, 2025, 0.0250 kg/s on September 14, 2025, 0.0417 kg/s on September 16, 2025, and 0.0500 kg/s on September 15, 2025. Fig. 11 illustrates the variations in solar radiation and ambient temperature recorded during these days. The results show typical behavior for sunny days. Solar radiation increases gradually during the morning until it reaches its maximum around midday, before decreasing thereafter. The

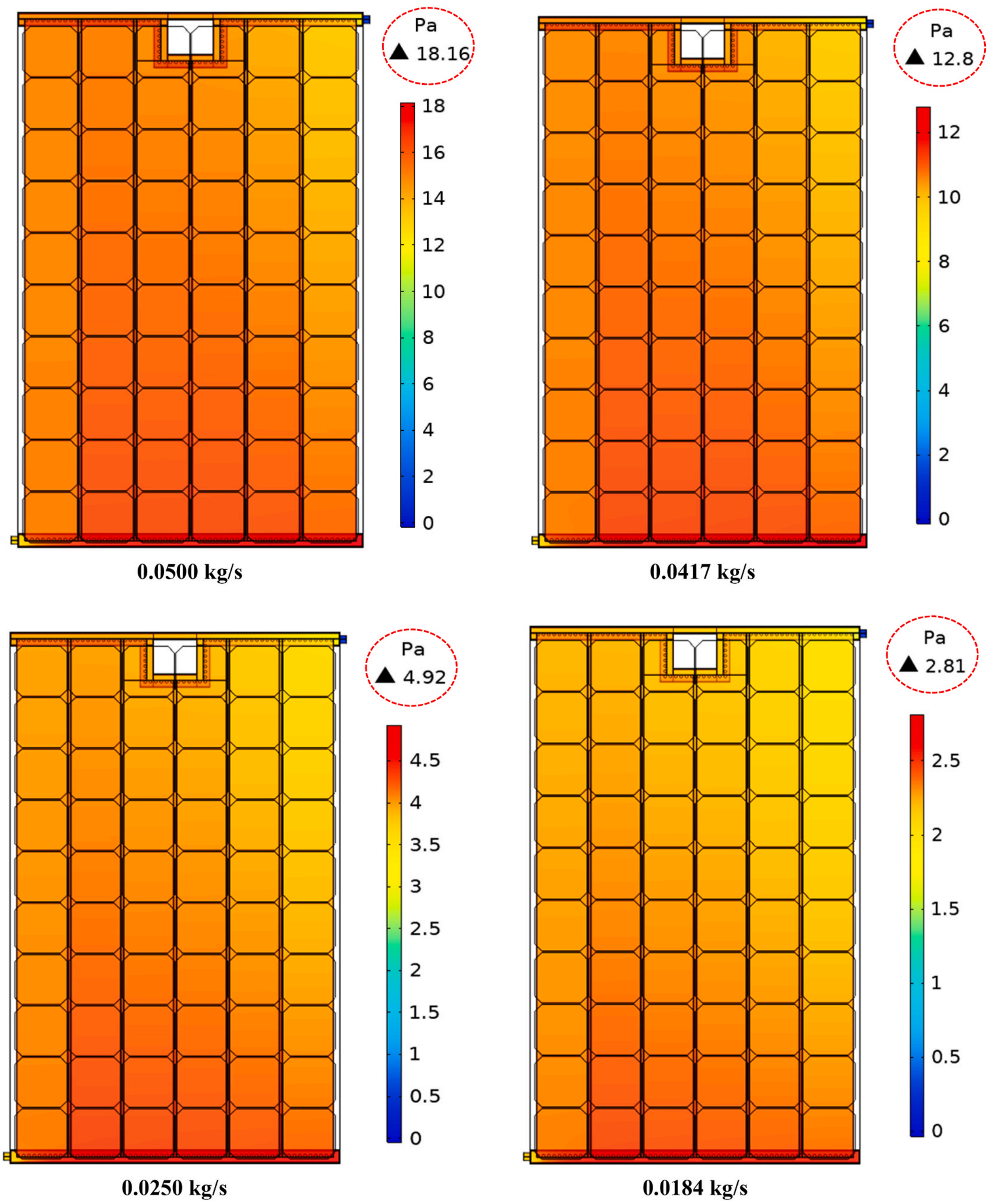

Fig. 14. Pressure distribution in the PVT-S for different MFRTs.

maximum values observed are 924.8 W/m^2 for a flow rate of 0.0183 kg/s, 955.7 W/m^2 for 0.0250 kg/s, 951.2 W/m^2 for 0.0417 kg/s, and 997.1 W/m^2 for 0.0500 kg/s, generally measured between 13h00 and 14h00. The ambient temperature changes in a similar way, with a gradual increase followed by a decrease after the peak of sunshine. The maximum temperatures recorded reached 30.7 °C, 33.8 °C, 34.2 °C, and 33.6 °C, respectively, depending on the flow rates tested, and these values were recorded between 12h 45 and 14h 15.

4.2. PVT temperature distribution and model validation

Fig. 12 illustrates the thermal distribution of PV cells obtained from numerical simulation of the PVT-S for different water flow rates studied. It can be observed that increasing the water flow rate significantly enhances heat dissipation, leading to a general decrease in cell temperature and a more uniform distribution across the entire module surface. When the fluid is introduced into the system, the PV cells are subjected to a significant cooling effect that is observed through a significant reduction in local temperature. Then, the fluid passes through the concentrator and absorbs the heat exuded by the panel, so that it itself gains temperature gradually and hence reduces its ability to effectively cool. As a result, a slight increase in the temperature of the PV cells is observed at the outlet. The results also show that the area corresponding to the junction box does not benefit from any heat exchange with the fluid. This lack of cooling leads to a concentration of the maximum temperature in this part of the panel. In general, for a higher flow rate of 0.0500 kg/s (Fig. 13a), the temperature distribution on the panel surface becomes significantly more uniform. This thermal uniformity minimizes local gradients, reduces thermal stresses on the photovoltaic material, improves the electrical and thermal efficiency of the panel, and mitigates the main performance and durability issues reported in the literature. A comparison between the numerical results and the experimental

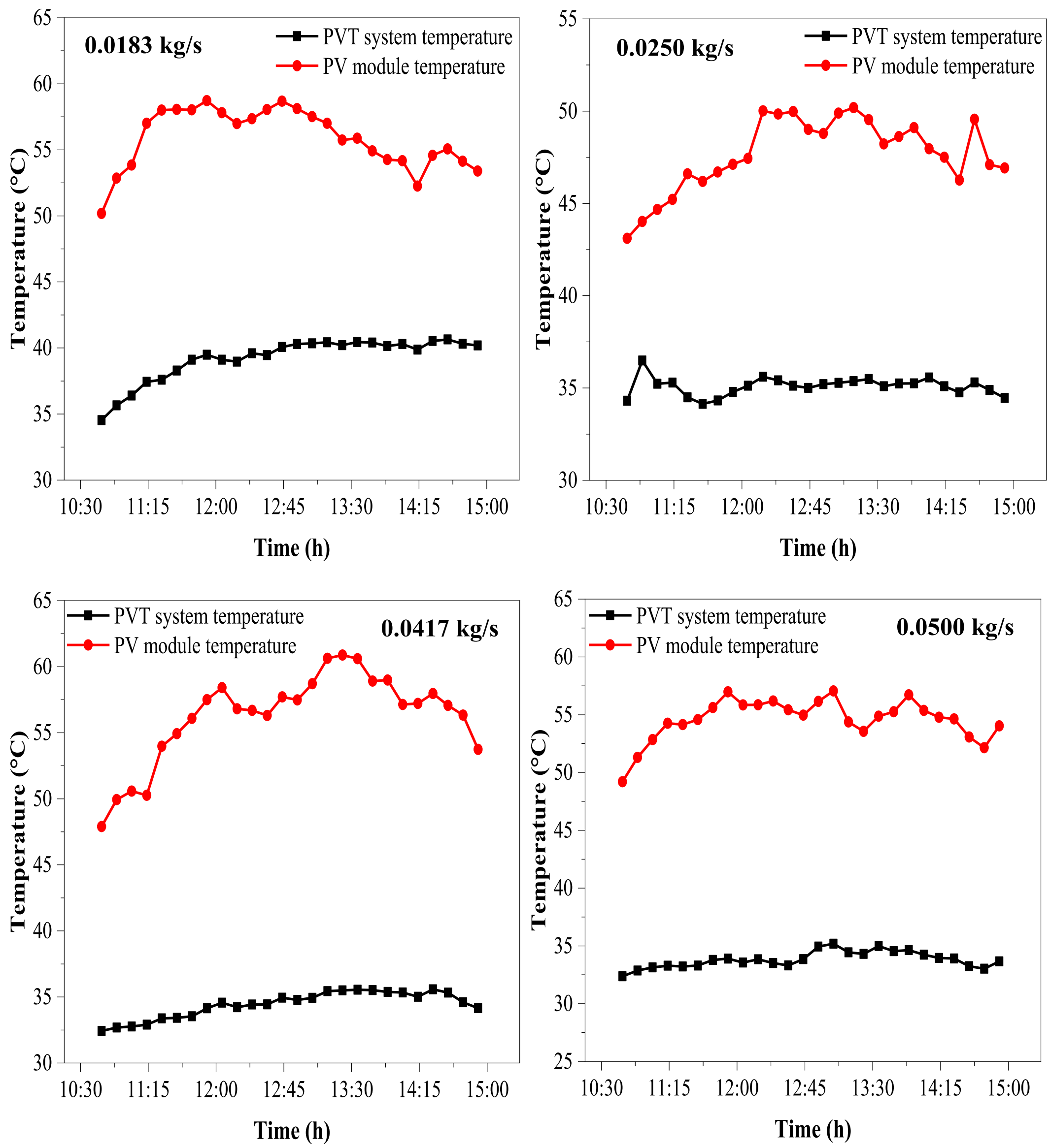

Fig. 15. Daily variation in PVT-S temperature compared to the reference PV panel for different MFRTs.

thermal images is shown in Fig. 13a and b reveal good agreement, both in terms of thermal gradients and the location of hot spots. Since thermal images only provide the extreme temperatures reached by the system, quantitative validation was performed by comparing the simulated and measured maximum temperatures. For an MFRT of 0.0184 kg/s, the absolute error on the maximum temperature is 0.69 °C, while it reaches 2.73 °C for a MFRT of 0.0500 kg/s. These small deviations confirm the good accuracy and robustness of the numerical model developed.

4.3. Pressure analysis

Fig. 14 illustrates the pressure distribution within the proposed PVT-S for various water flow rates. The maximal pressure found at the sensor inlet is explained by the high flow velocity imposed at this point. As it progresses along the channel, the pressure gradually decreases until it reaches the outlet, reflecting the normal pressure losses induced by the flow in the conduit. The analysis also shows that the pressure increases with the MFRT. For low MFRT 0.0184 kg/s, the maximum pressure reaches only 2.81 Pa, while at a higher MFRT 0.0500 kg/s, it rises to 18.16 Pa. Despite rising MFRT, the recorded values remain very low, highlighting the robustness and hydraulic efficiency of the proposed new system. These pressure levels are significantly lower than those reported in other PVT-S designs studied previously. Poredoš et al. [28], Kazemian et al. [54], and Karaaslan et Menlik [55] obtained pressure drop values of 778 Pa, 874 Pa, and 214.78 Pa, respectively. These results are a clear indication of the fact that the newly proposed design incurs significantly less pressure losses and has a significantly better hydraulic performance.

4.4. Analysis of temperature

The evolution of the temperature of the PVT-S compared to that of the reference PV module during the measurement days corresponding to each MFRT studied is shown in Fig. 15. The results demonstrate that the temperature of the PVT-S remains consistently lower than that of the reference PV panel. This difference can be attributed to the cooling effect provided by the circulation of the heat transfer fluid. In particular, at an MFRT of 0.0183 kg/s, the maximum temperature of the PVT-S reaches 40.65 °C, while the reference PV module reaches a maximum temperature of 58.72 °C. In fluid dynamics and thermal performance analysis, increasing the flow rate to 0.0250 kg/s lowers the maximum temperature of the PVT-S to 36.49 °C, while the PV panel reaches 50.19 °C.

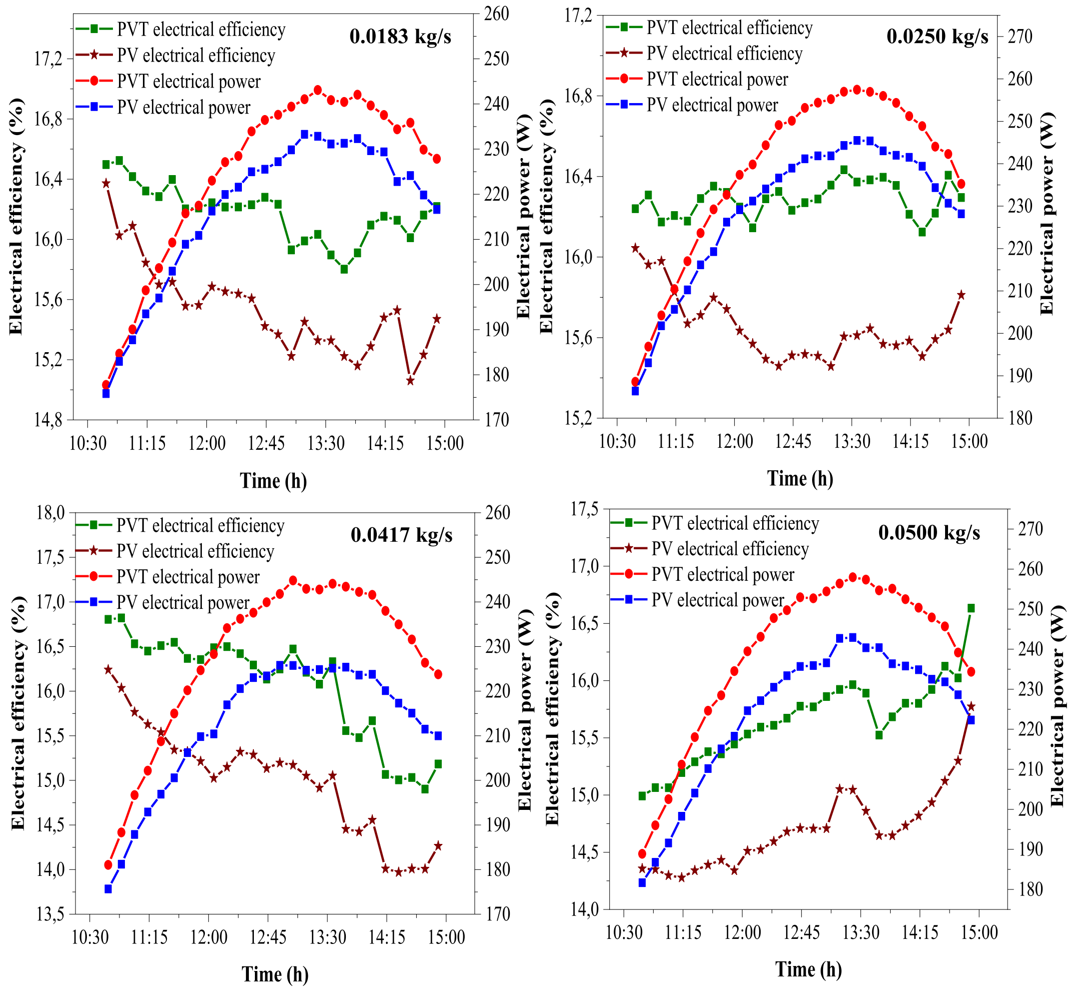

Fig. 16. Daily variation in electrical power and efficiency of the PVT-S compared to the reference PV panel for different MFRTs.

Higher flow rates of 0.0417 kg/s and 0.0500 kg/s further decrease the PVT-S temperatures to 35.58 °C and 35.19 °C, with PV panel temperatures at 60.88 °C and 57.05 °C, respectively. These results highlight the conclusive link between flow rate and temperature drop, demonstrating the importance of flow rate control in optimizing the TEF of solar energy systems. The study shows an inverse relationship between the temperature of the PVT-S and the increasing MFRT. The highest temperature differences measured between the PVT-S and the reference PV panel were 20.41 °C, 14.86 °C, 25.38 °C, and 23.08 °C, depending on the flow rates used. These results confirm the system's capacity to cool the temperature of PV cells, thereby increasing their efficiency and durability.

4.5. Analysis of the power and electrical efficiency

Fig. 16 compares the electrical power and efficiency of the PVT-S to a reference PV panel at various MFRTs. The PVT-S consistently outperforms the PV panel. At MFRT 0.0183 kg/s, the PVT-S achieves a maximum power output of 243.07 W and an efficiency of 16.52%. In contrast, the PV panel produces 233.25 W with an efficiency of 16.37%. At a higher MFRT 0.0250 kg/s, the PVT-S reaches 257.45 W and an efficiency of 16.43%, while the PV panel generates 245.48 W and an efficiency of 16.04%. At MFRT 0.0417 kg/s, the PVT-S displays 244.79 W and 16.82%, compared to 225.78 W and 16.24% for the PV panel. Finally, for MFRT 0.0500 kg/s, the maximum power and efficiency of the PVT-S are 257.95 W and 16.63%, respectively, while the reference PV panel records 242.91 W and 15.77%. The comparative analysis shows that increasing the MFRT tends to improve the power and efficiency, although the effect is not strictly linear, as it also depends on variations in irradiance and ambient temperature. The maximum differences observed between the PVT-S and the PV panel are 11.68 W and 0.94% for 0.0183 kg/s, 13.37 W and 0.89% for 0.0250 kg/s, 19.03 W and 1.46% for 0.0417 kg/s, and 17.82 W and 1.15% for 0.0500 kg/s.

4.6. Analysis of inlet-outlet temperatures, and thermal efficiency

The evolution of the fluid inlet and outlet temperatures, as well as the TEF, during tests carried out for different MFRTs is illustrated in Fig. 17. The inlet temperature is relatively steady under all experimental conditions and is in the range of 24 °C 26 °C and therefore reflects a constant supply of circuit during the measurements. On the contrary, the temperature of the outlet is also highly variable with the flow rate used. For MFRT 0.0183 kg/s, the outlet temperature reaches 35.75 °C, then gradually decreases to 33.00 °C for 0.0250 kg/s, 32.25 °C for 0.0417 kg/s, and 31.25 °C for 0.0500 kg/s. This decrease in outlet temperature with increasing MFRT is explained by the fact that the higher the fluid velocity, the more it is able to capture thermal energy from the panel. An increased MFRT reduces the time period during which the fluid can flow through the channel, thereby limiting the internal heat generation of the channel and, at the same time, increasing the overall heat transfer efficiency. The evolution of TEF confirms this trend. The maximum values reach 59.92% for 0.0183 kg/s, 60.17% for 0.0250 kg/s, 75.84% for 0.0417 kg/s, and 78.90% for 0.0500 kg/s. The average efficiencies recorded are 41.48%, 49.73%, 59.78%, and 55.65%, respectively. These values are non-linear, and this effect can be attributed to variability of

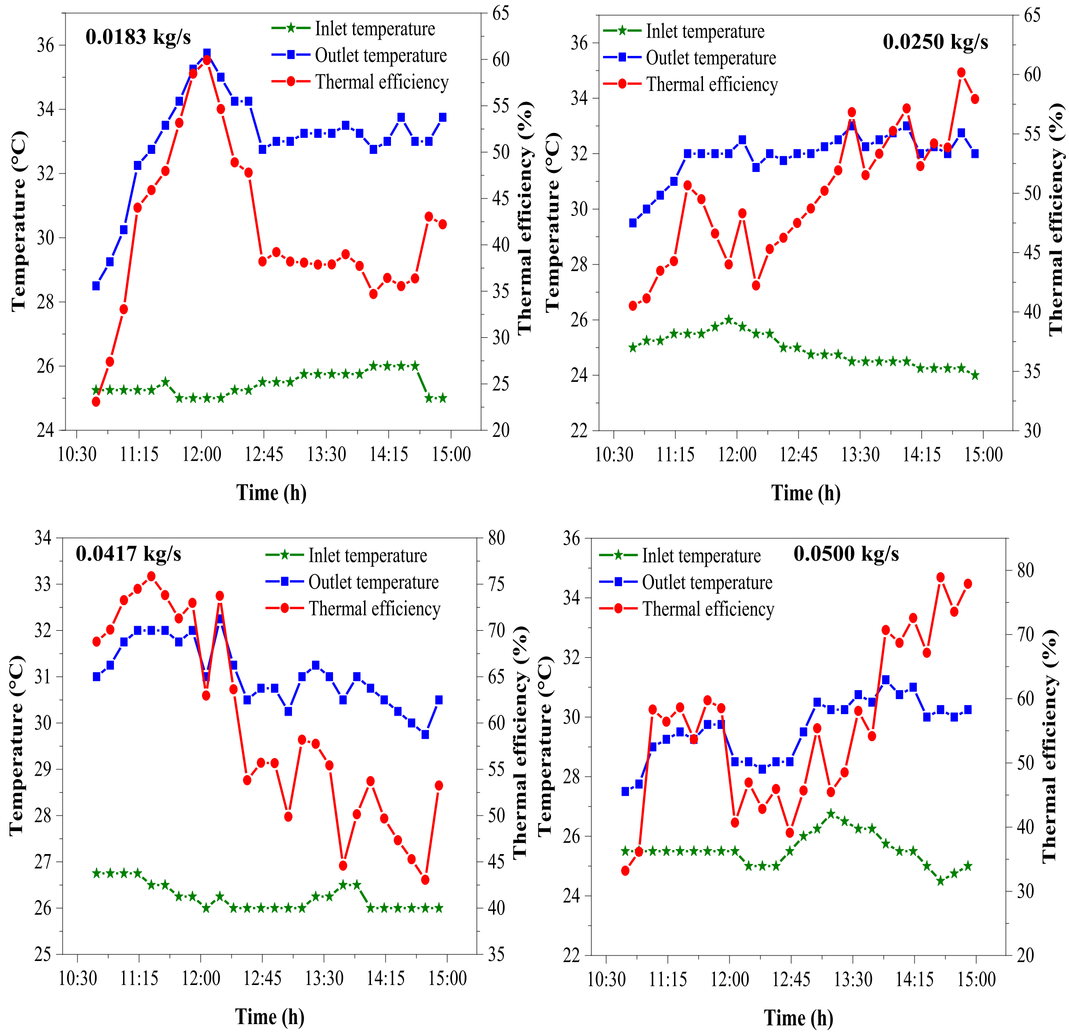

Fig. 17. Daily variation in fluid inlet and outlet temperatures and TEF against MFRTs.

the external environment, which includes solar radiation, ambient temperature, and little fluctuation in inlet temperature that occurs continuously within the span of a testing day.

4.7. Analysis of overall electrical and exergy efficiency

Fig. 18 shows the evolution of EEF and total exergy efficiency during the experimental day for different heat transfer fluid MFRTs. The maximum total electrical efficiencies reach 76.16%, 76.58%, 92.35%, and 95.03% for MFRTs of 0.0183, 0.0250, 0.0417, and 0.0500 kg/s, confirming the beneficial effect of increasing the flow rate on the cooling of the PV panel and, consequently, on improving electrical conversion. The average electrical efficiencies obtained, i.e., 57.66%, 66.01%, 75.83%, and 71.30%, reflect the overall stability of the performance of the proposed PVT-S. This improvement is mainly due to the system configuration, which ensures direct contact between the heat transfer fluid and the rear surface of the module, promoting efficient heat extraction and limiting the temperature rise of the cells. From an exergy perspective, the maximum total exergy efficiencies recorded are 17.56%, 16.63%, 17.16%, and 16.10% for the same MFRT. Unlike the evolution of EEF, the variation in exergy efficiency remains moderate with increasing flow rate, which can be explained by the qualitative nature of thermal exergy, which is highly dependent on the temperature difference between the fluid and the environment. In fact, increasing the flow rate improves heat extraction but tends to reduce the average temperature of the outlet fluid, thereby decreasing the exergy quality of the recovered thermal energy. Consequently, the total exergy of the system is a compromise between the improvement in electrical production due to module cooling and the relative decrease in the thermal exergy contribution at high flow rates.

4.8. Analysis of exergy destruction and entropy generation

Entropy generation and exergy destruction are significant indicators of the strict evaluation of exergy efficiency of PVT-Ss. The elimination of these thermodynamic losses is invaluable to the enhancement of the operation of the thermal processes, as it has a significant impact on the total efficiency and effectiveness. Based on this, systematic mitigation of these losses not only increases the energy production but also adds to the greater goal of ensuring sustainability in thermal energy utilization. Fig. 19 illustrates the evolution of these two parameters for the four MFRTs studied, compared with a reference PV panel. For all flow rates, these two parameters increase with solar irradiance and reach their maximum value around noon, the period corresponding to the most intense radiation. In all cases, the values measured for the reference PV panel remain higher than those of the PVT-S. For example, for a flow rate of 0.0183 kg/s, the average exergy destruction and entropy generation of the PV panel are 1091.41 W and 3.614 W/°C, respectively, compared to 1074.36 W and 3.558 W/°C for the PVT-S. For 0.0250 kg/s, these values are 1146.03 W and 3.756 W/°C for PV and 1137.06 W and 3.727 W/°C for PVT-S. At 0.0417 kg/s, they are 1122.38 W and 3.680 W/°C for PV and 1110.29 W and 3.640 W/°C for PVT-S, while at 0.0500 kg/s, they

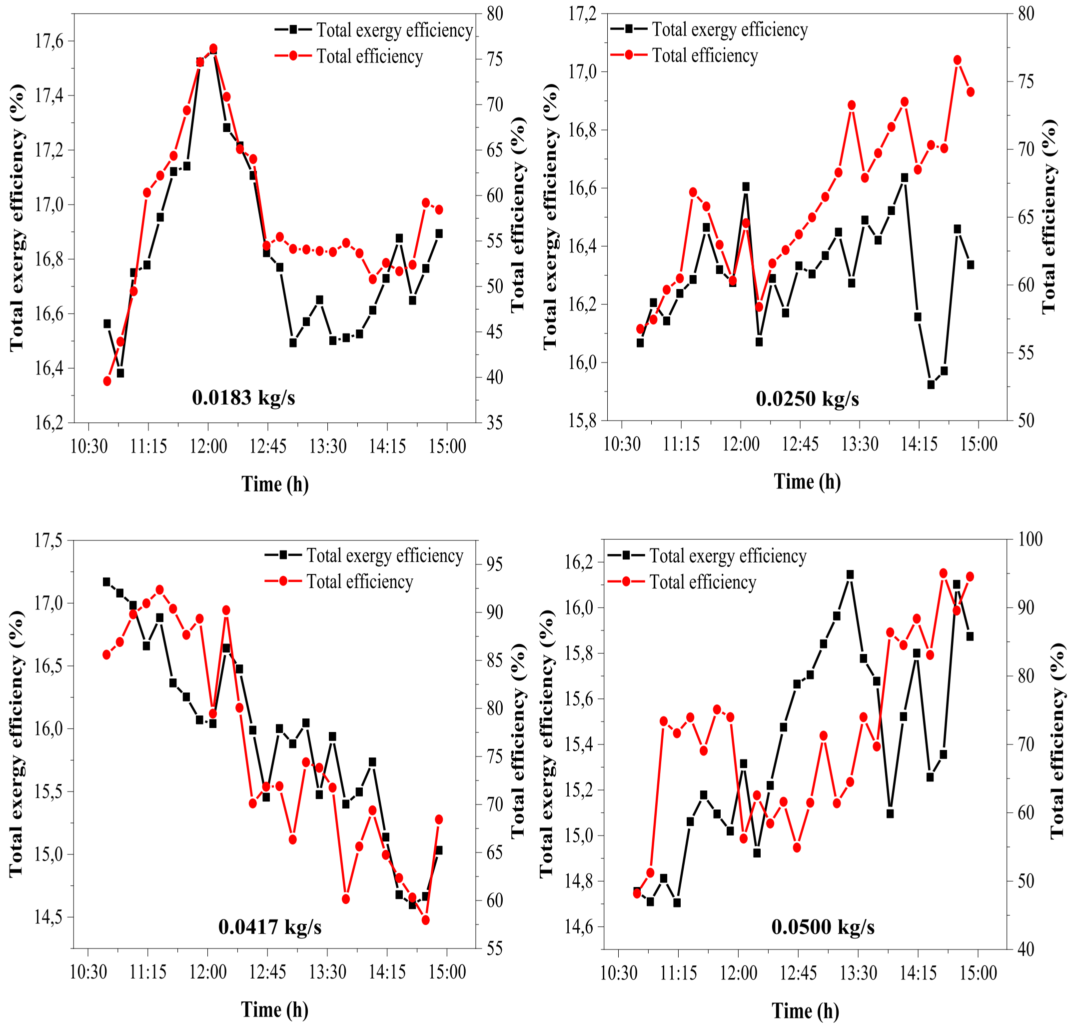

Fig. 18. Daily variation in EEF and total exergy efficiency versus MFRTs.

reach 1206.44 W and 3.967 W/°C for PV and 1196.54 W and 3.935 W/°C for PVT-S. The enhanced performance of the reference PV panel is due to its lack of active cooling mechanisms. Unlike the PVT-S, which circulates a heat transfer fluid to manage temperature, the reference PV panel traps more thermal energy. This leads to greater exergy losses and increased entropy. The PVT-S reduces heat buildup, improving the exergy efficiency of the system. This comparison emphasizes the importance of thermal management in optimizing PV technologies.

4.9. Analysis of open-circuit voltage and short-circuit current

Fig. 20 shows the variation in voltage and electric current for the PVT-S and the reference PV panel throughout the day for different MFRTs. It can be seen that the voltage of the PVT-Ss is consistently higher than that of the reference PV for all flow rates, highlighting the beneficial effect of active cooling. For a flow rate of 0.0183 kg/s, the average voltage of the PVT-S is 31.03 V, compared to 29.10 V for the PV, resulting in a difference of 1.92 V. At a flow rate of 0.0250 kg/s, this difference is 1.35 V (31.33 V for PVT-S and 29.98 V for PV). At 0.0417 kg/s, the average voltage is 31.41 V for the PVT-S and 28.72 V for the PV, with a difference of 2.68 V. Finally, at 0.0500 kg/s, the average voltage of the PVT-S is 31.77 V compared to 29.46 V for the PV, a difference of 2.31 V. These values show that increasing the MFRT slightly improves cooling efficiency and maintains a higher voltage, limiting cell overheating. On the other hand, the electric current seems to be less influenced by cooling and more by solar radiation. Although the PVT-S benefits from cooling, the highest current was observed for the reference PV, indicating that solar irradiance remains the dominant factor for current. This difference is particularly noticeable around noon, when solar radiation and ambient temperature are at their maximum.

4.10. Analysis of sustainability factors

Fig. 21 shows the evolution of the PVT-S's sustainability indicators for different heat transfer fluid MFRTs. Fig. 21a shows that the sustainability index (SI) varies slightly with flow rate, reflecting the balance between improved energy performance and reduced thermodynamic irreversibilities. The maximum values obtained are 1.21311 for 0.0183 kg/s, 1.19956 for 0.0250 kg/s, 1.20728 for 0.0417 kg/s, and 1.19193 for 0.0500 kg/s, indicating that the system maintains relatively stable, sustainable performance despite the increase in flow rate, confirming efficient use of available energy. This trend is consistent with the variations in the waste exergy ratio (WER) shown in Fig. 21b. The intervals observed, ranging from 0.83618 to 0.82433, 0.84077 and 0.83364, 0.85402 and 0.82831, and between 0.85296 and 0.83855, show that the proportion of unutilized exergy remains significant but relatively stable. This suggests that increasing the flow rate improves heat extraction while generating exergy losses due to lower temperature gradients, which limits the significant reduction in irreversibilities. Fig. 21c shows that the improvement potential (IP) increases with solar irradiance and MFRT, reaching maximum values of 986.754 W, 1019.417 W, 1059.402 W, and 1089.478 W for the flow rates studied. This trend highlights that,

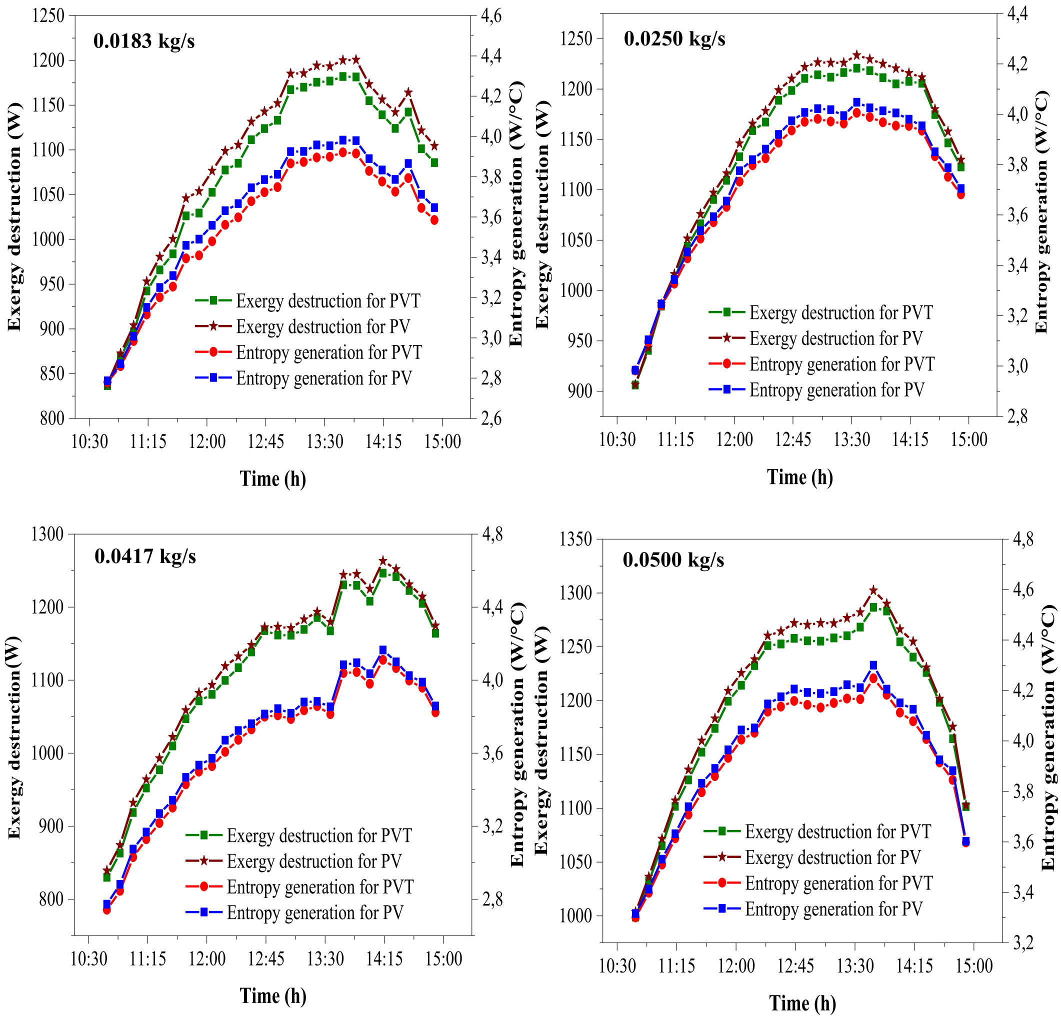

Fig. 19. Daily variation in exergy destruction and entropy generation for PVT-S and reference PV against MFRT.

despite the system's satisfactory performance, there is still room for optimization, particularly in terms of thermal management and heat exchanger design, in order to reduce exergy destruction. Finally, Fig. 21d shows the evolution of the ecological exergy indicator (EcEI), which assesses the overall efficiency of exergy resource use. The negative values observed, reaching −0.64865, −0.66728, −0.65661, and −0.67710, respectively, indicate that the share of non-useful exergy remains dominant, reflecting a still significant exergy degradation of the system. Nevertheless, the slight variation in this indicator with flow rate suggests that the overall environmental performance of the PVT-S remains relatively stable over the operating range studied. Table 7 completes this analysis by comparing the sustainability indicators obtained with those reported in the literature, thus allowing the performance of the proposed system to be compared with previous work and confirming its potential in terms of energy and environmental sustainability.

4.11. Comparison

To assess our system's efficacy, we compared our results with existing literature on the overall electrical, thermal, and exergy efficiencies of PVT-Ss, summarized in Table 8. Previous studies indicate that the TEF of PVT-Ss ranges from 26.87% to 76.50%, providing a benchmark for our performance. These differences cannot be explained solely by the simple effect of panel cooling. Several parameters strongly influence performance, including local climatic conditions, solar irradiation levels, the cooling strategy adopted, the heat transfer fluid flow rate, and the manufacturing and assembly methods of the PVT-S. The combination of these factors makes any direct comparison complex. In our study, the PVT-S designed achieved a maximum TEF of 78.90%, confirming the efficiency and robustness of our PVT-S.

5. Conclusions

A new PVT-S was proposed and assessed both numerically and experimentally across various MFRTs. Its performance was examined in terms of energy and exergy, pressure drops, temperature distribution, exergy loss, and entropy production. Several sustainability indicators were also considered, including the sustainability index, Waste Exergy Ratio, potential for improvement, and ecological efficiency index. The main results obtained are as follows.

- Comparison between the numerical and experimental results shows a strong correlation in thermal distribution, authorizing the simulation's steadfastness.
- The PVT-S developed offers more uniform heat distribution than the flat plate PVTs reported in the literature, with low pressure losses of 18.16 Pa at 0.0500 kg/s MFRT.
- The increase in MFRT leads to a gradual decrease in the temperature of the PVT-S. At a flow rate of 0.0183 kg/s, the maximum temperature of the PVT-S is 40.65 °C, while the reference PV panel reaches 60.88 °C at 0.0417 kg/s. This results in a maximum temperature difference of 25.38 °C between the two systems.

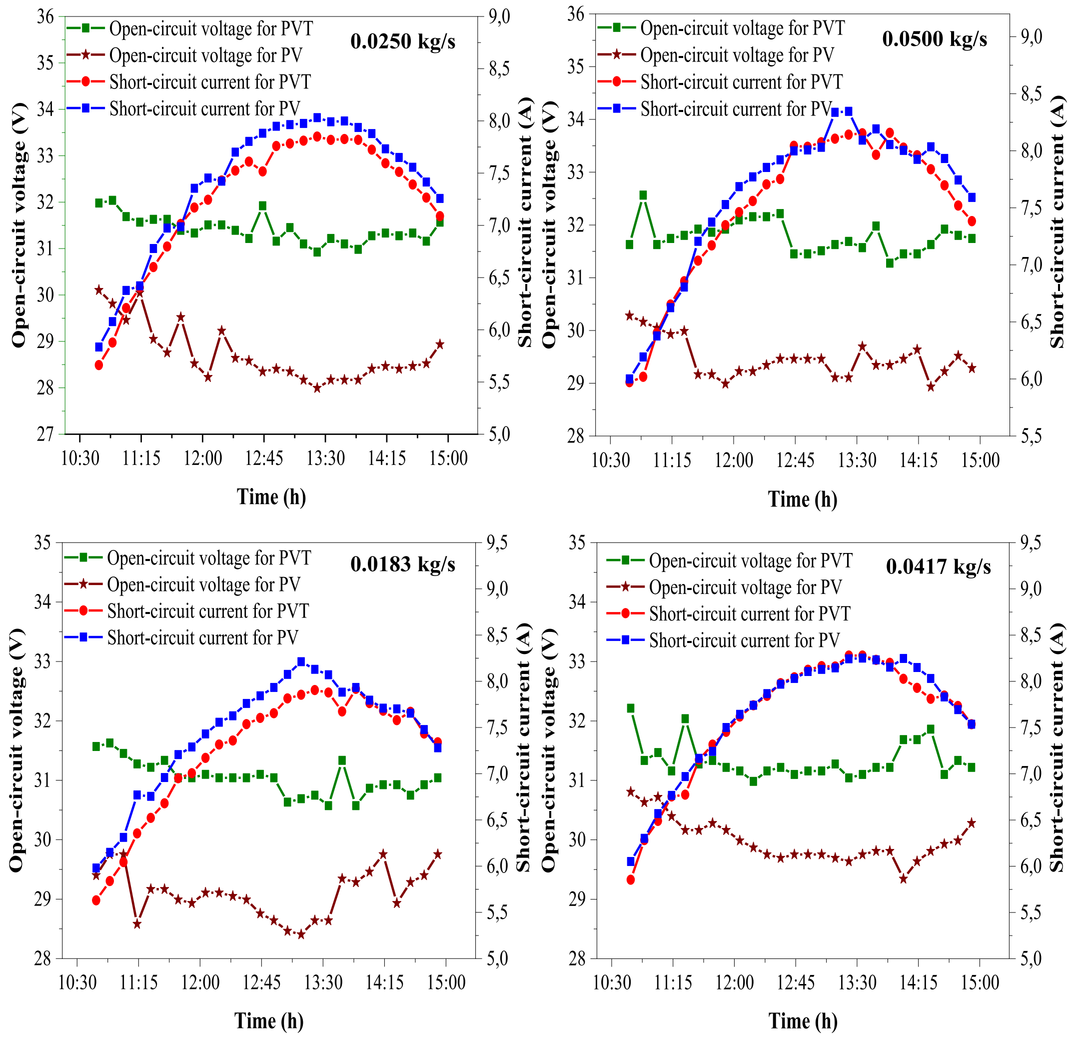

Fig. 20. Daily variation in electrical voltage and current of the PVT-S compared to the reference PV module for different MFRTs.

- The PVT-S has a maximum electrical power and efficiency of 257.95 W and 16.82%, obtained respectively for MFRT 0.0500 kg/s and 0.0417 kg/s. Conversely, the reference PV panel records minimum values of 225.78 W and 15.77% for the same flow rates. The maximum difference observed between the two systems is thus 19.03 W for power and 1.46% for efficiency at a flow rate of 0.0417 kg/s.
- The fluid outlet temperature decreases from 35.75 °C to 31.25 °C for increasing MFRT ranging from 0.0183 kg/s to 0.0500 kg/s. At the same time, the TEF of the system improves as the flow rate increases. Maximum thermal efficiencies reach 59.92%, 60.17%, 75.84%, and 78.90% for MFRT 0.0183, 0.0250, 0.0417, and 0.0500 kg/s, respectively, while the corresponding average efficiencies are 41.48%, 49.73%, 59.78%, and 55.65%.
- The PVT-S system exhibited an average total EEF of 75.83% at a flow rate of 0.0417 kg/s and a maximum total exergy efficiency of 17.56% at 0.0183 kg/s. Additionally, the highest exergy destruction and entropy generation were recorded at 1196.54 W and 3.935 W/°C, respectively, at a flow rate of 0.0500 kg/s.
- The PVT-S has a maximum sustainability index (SI) of 1.21311 for a flow rate of 0.0183 kg/s. The Waste Exergy Ratio (WER) reaches its maximum value of 0.85402 at MFRT 0.0417 kg/s. The improvement potential (IP) increases with solar irradiance and MFRT, reaching a maximum value of 1089.47 W for MFRT 0.0500 kg/s. Finally, the maximum Ecological Exergy Indicator (EcEI) observed is −0.64865 for a flow rate of 0.0183 kg/s.

Despite the reliability of the proposed new system, certain limitations remain. The experimental conditions were limited to El Jadida, which means that the results are only valid for the specific climate of that city and could lead to variations in other climatic conditions. Furthermore, as this is the first time this system has been proposed and studied, the tests were carried out over a limited period, which does not allow for an assessment of the system's long-term performance or the effect of material wear and tear. Finally, the observed performance depends on the design and materials chosen for the exchanger and panel, which may limit its generalizability to other PVT-Ss.

6. Future work

The new PVT-S presented in this study fills several gaps identified in the existing literature and thus opens up new avenues for future research. Given that the working fluid comes into direct contact with the PV panel, a rigorous evaluation of alternative fluids, particularly nanofluids, should be considered, as these can increase the efficiency of the thermal cycle and electrical power. In addition, the effects of prolonged contact between the fluid and the panel on the longitudinal behavior and structural integrity of the PV cells need to be investigated. Evaluation of the system during each of the climatic seasons is also urgent, as it will allow for the assessment of annual performance indicators and the determination of the period during which optimal energy can be obtained. Finally, additional experimental and computational studies can explore the sensitivities of panel geometry, heat exchanger

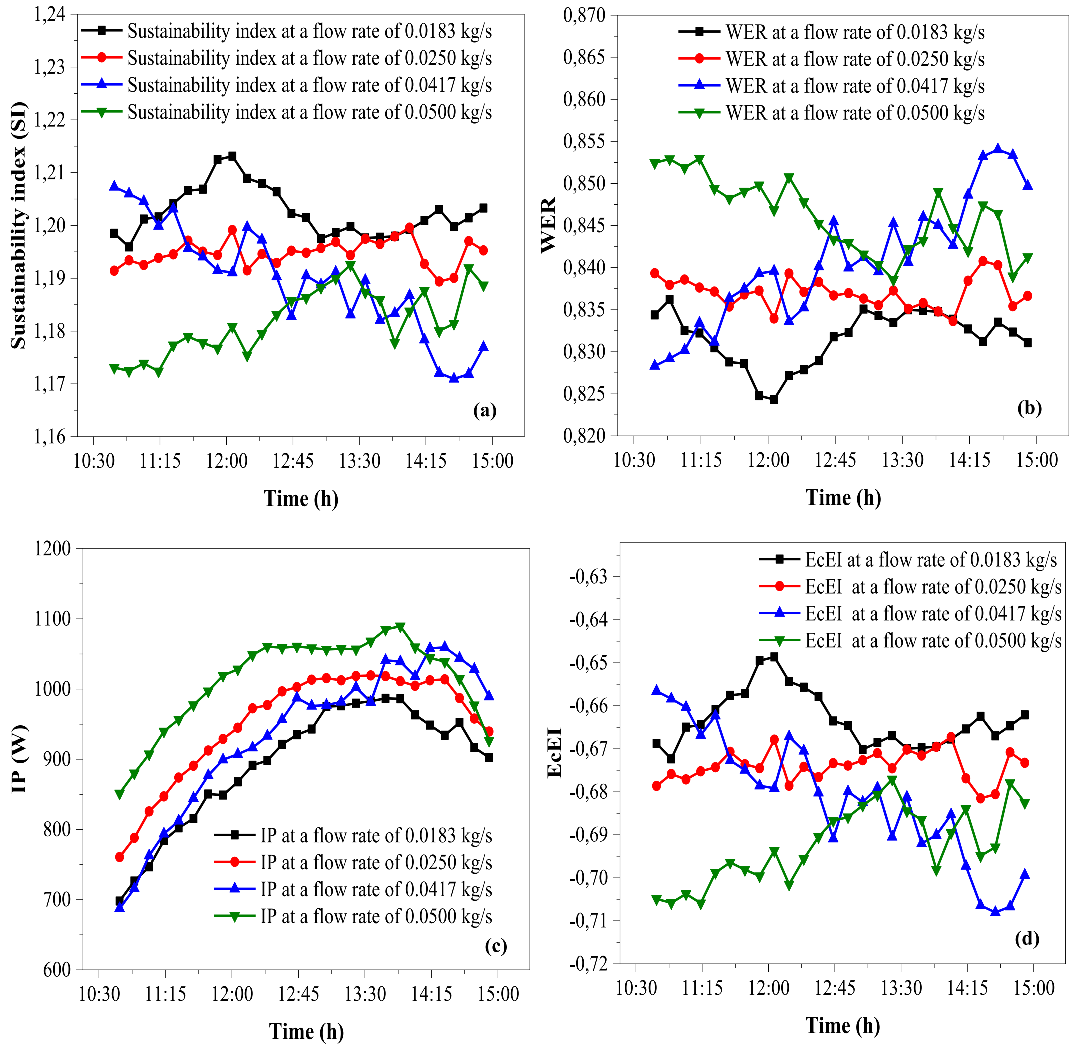

Fig. 21. Daily variation in PVT-S sustainability indicators: (a) SI, (b) WER, (c) IP, and (d) EcEI.

Table 7
Comparison of the four PVT-S sustainability indicators for an MFRT of 0.0183 kg/s with the results published in the literature.

References &year	Type of PVT-S	SI	WER	EcEI	IP
[56], 2022	Air-based PVT-S	1.147-1.174	NA	NA	351.92-368.84
[57], 2023	Air-based Model-∇ system	1.141-1.157	NA	NA	119.09-329.24
[58], 2024	Water-based PVT-S	1.04-1.08	0.935-0.968	−0.92-(-0.86)	68-75.5
[45], 2024	PVT-S with rectangular channel	1.172-1.186	0.843-0.854	−0,707-(-0,687)	215,647–421,145
[59], 2024	PV panel integrated with a heat pump for drying applications	2.327	0.83	NA	0.145
Present study	Direct water–PV contact PVT-S	1195–1213	0,824–0,836	−0,672 – (−0,648)	697,912–986,754

components, and localized climatic variations, thereby enabling the development of more flexible design calibrations and improving the reliability of PVT-S.

CRediT authorship contribution statement

Yassine El Alami: Writing – original draft, Methodology, Investigation, Formal analysis, Data curation, Conceptualization. **Hicham El Achouby:** Writing – review & editing, Methodology, Formal analysis, Conceptualization. **Rehena Nasrin:** Writing – review & editing, Validation, Data curation, Conceptualization. **Charaf Hajjaj:** Writing – review & editing, Validation, Data curation, Conceptualization. **Mohammadi Benhmida:** Writing – review & editing, Validation, Data curation, Conceptualization. **Elhadi Baghaz:** Writing – review & editing, Validation, Data curation, Conceptualization. **Mohammed Ghazal:** Writing – review & editing, Validation, Methodology, Funding acquisition, Formal analysis, Conceptualization. **Adnan Ibrahim:** Writing – review & editing, Validation, Supervision, Methodology, Funding acquisition, Formal analysis, Conceptualization.

Funding declaration

This research received no specific grant from any funding agency in the public, commercial, or not-for-profit sectors.

Declaration of competing interest

The authors declare that they have no known competing financial interests or personal relationships that could have appeared to influence the work reported in this paper.

Table 8
Comparison of energy and exergy yields of new PVT-S with literature.

References &year	Study type	Fluid type	η_{el} (%)	η_{th} (%)	ε_{PVT} (%)
[60], 2024	Experimental	Bi-symmetrical	18.01	63.09	21.15
[61], 2024	Experimental	Serpentine tube	11.8	32.79	12.21
[62], 2025	Numerical	Wavy collector Tube	11.82	75.32	14.67
[39], 2025	Numerical	Serpentine tube	13.9	44.4	14.4
[63], 2020	Experimental	Serpentine tubes	12.1	32.9	13.5
[64], 2024	Experimental	sheet-and-tube absorber	12.80	43.16	14.0
[65], 2019	Experimental	sheet-and-tube absorber	14.6 -17.1	63.1	11.2-20.6
[66], 2019	Experimental	Serpentine tube	17.33	26.87	14
[67], 2025	Experimental	Plate-fin heat exchanger	15.40	76.50	12.50
Present study	Experimental	Direct water–PV contact PVT-S	16,43-16,82	59,92-78,90	16,10-17,56

Data availability

Data will be made available on request.

References

[1] Azeez HL, Ibrahim A, Ahmed BO, Dol SS, Al-Waeli AHA, Jaber M. Experimental evaluation of a novel photovoltaic thermal system: energy, economic, and exergy-based sustainability analysis. Case Stud Therm Eng 2025;71:106167. https://doi.org/10.1016/j.csite.2025.106167.

[2] Alami YE, Baghaz E, Nasrin R, Hajjaj C, Benhmida M, Al-Aribe KM, et al. Numerical exploration and relational impact ranking of critical parameters in 3D PV module studies. Results Eng 2025:107097. https://doi.org/10.1016/j.rineng.2025.107097.

[3] El Alami Y, Achouby HE, Baghaz E, Hajjaj C, Nasrin R. An innovative photovoltaic thermal system with direct water-cell contact: energy, exergy, and sustainability analysis. Sol Energy 2025;300:113827. https://doi.org/10.1016/j.solener.2025.113827.

[4] El Alami Y, Rami M, Hajjaj C, Benhmida M, Faize A, Baghaz E. Three-dimensional thermal modeling and analysis of the heat source, the impact of encapsulation materials and the back sheet of silicon PV modules. Appl Therm Eng 2025;280:128430. https://doi.org/10.1016/j.applthermaleng.2025.128430.

[5] Mirza CR, Alsharifi T, Mahdi JM, Taqi Al-Najjar HM, Zayani HM, Ben Khedher N. Efficient thermal management of PVT systems via water-PCM hybridization: new design with optimized geometrical configuration. Appl Therm Eng 2025;280:128431. https://doi.org/10.1016/j.applthermaleng.2025.128431.

[6] Hudişteanu V-S, Cherecheş N-C, Ţurcanu F-E, Hudişteanu I, Romila C. Impact of temperature on the efficiency of monocrystalline and polycrystalline photovoltaic panels: a comprehensive experimental analysis for sustainable energy solutions. Sustainability 2024;16:10566. https://doi.org/10.3390/su162310566.

[7] Bady M, Attia MEH, Khelifa A, Kabeel AE. Investigating the effect of cooling tower height on PVT system efficiency with a four-inlet air cooling: energy and exergy analysis. Int J Refrig 2025;177:207–18. https://doi.org/10.1016/j.ijrefrig.2025.05.029.

[8] Hasan AA, Abdullah Md, Sazid AS. A computational analysis of air-cooled heat sinks designs for PV solar panel cooling with different fin numbers. Heat Transf 2025;54:1462–75. https://doi.org/10.1002/htj.23236.

[9] El Alami Y, Ameur A, Benhmida M, Rabhi A, Baghaz E. Performance evaluation of different new channel box photovoltaic thermal systems. J Clean Prod 2024;478:143953. https://doi.org/10.1016/j.jclepro.2024.143953.

[10] Alsharifi T, Sultan Aljibori HS, Mahdi JM. Design optimization and performance evaluation of a photovoltaic/thermal collector with porous twisted tape inserts: a comprehensive energy and exergy analysis. Int Commun Heat Mass Transf 2024;159:108104. https://doi.org/10.1016/j.icheatmasstransfer.2024.108104.

[11] Basuhaib A, Selvaraj J, Hasanuzzaman M, Anjum T, Kumar L. Experimental investigation the effect of different operating parameters and optimized the water-based PVT system for domestic applications. Sol Energy 2024;268:112278. https://doi.org/10.1016/j.solener.2023.112278.

[12] Moein-Jahromi M, Aboueian J. PCM-based annular flow for enhanced thermal management of PV/T units. Energy Convers Manag 2025;344:120304. https://doi.org/10.1016/j.enconman.2025.120304.

[13] El Alami Y, Baghaz E, Bendaoud R, Chanaa F, Benhmida M, Ezzaki H, et al. Experimental-numerical investigation of the photovoltaic thermal system with polypropylene heat exchanger: case in Morocco. IET Renew Power Gener 2025;19:e70041. https://doi.org/10.1049/rpg2.70041.

[14] Al-Mamoori ZMS, Kilinc E. Numerical investigation to improve thermal performance of a water-cooling PVT collector with novel cooling subchannels. Sci Rep 2025;15:34317. https://doi.org/10.1038/s41598-025-12938-z.

[15] Phukaokaew W, Suksri A, Punyawudho K, Wongwuttanasatian T. Optimisation of flow configuration for PVT system assisted by MgO nanoparticles PCM cooling. Energy Nexus 2025;17:100389. https://doi.org/10.1016/j.nexus.2025.100389.

[16] Maseer MM, Ismail FB, Kazem HA, Hachim DM, Abdulkareem Hadi al-Gburi K, Mahmoud ALShurafa S. Enhanced photovoltaic/thermal systems with innovative collector designs. Int J Green Energy 2025;22:3436–47. https://doi.org/10.1080/15435075.2025.2516816.

[17] Zhang Y, Zhao Y, Zhang H, Cheng C, Gao D, Chen H, et al. Numerical optimization and performance study of a photovoltaic/thermal module based on multi-stage V-type turbulators. Renew Energy 2025;252:123559. https://doi.org/10.1016/j.renene.2025.123559.

[18] Satpute J, Srinidhi C, Rathore SS, Yadav SM, Kumar A, Gajbhiye A, et al. Parametric influence and efficiency assessment of water-cooled photovoltaic thermal PV/T absorber designs. Energy 2025;320:135218. https://doi.org/10.1016/j.energy.2025.135218.

[19] Zhang D, Zhou Y, Yu Z, Ma T, Wang X. Experimental study on electricity generation performance of T-type direct-expansion solar PVT heat pump system. Eng Rep 2024;6:e13013. https://doi.org/10.1002/eng2.13013.

[20] Sheikholeslami M, Khalili Z. Solar photovoltaic-thermal system with novel design of tube containing eco-friendly nanofluid. Renew Energy 2024;222:119862. https://doi.org/10.1016/j.renene.2023.119862.

[21] Hosouli S, Bagde S, Talha Jahangir M, Hasnain Qamar S, Formosa N, Gomes J. Mitigating PV cell cracking in solar photovoltaic thermal collectors with a novel H-pattern absorber design. Appl Therm Eng 2024;242:122516. https://doi.org/10.1016/j.applthermaleng.2024.122516.

[22] Umam MF, Hasanuzzaman M, Abd Rahim N. Experimental investigation and performance evaluation of spiral and serpentine collectors based photovoltaic thermal system in Peninsular Malaysia. Sustain Energy Technol Assess 2023;58:103373. https://doi.org/10.1016/j.seta.2023.103373.

[23] Hossain MS, Pandey AK, Selvaraj J, Abd Rahim N, Rivai A, Tyagi VV. Thermal performance analysis of parallel serpentine flow based photovoltaic/thermal (PV/T) system under composite climate of Malaysia. Appl Therm Eng 2019;153:861–71. https://doi.org/10.1016/j.applthermaleng.2019.01.007.

[24] Yu C, Li H, Chen J, Qiu S, Yao F, Liu X. Investigation of the thermal performance enhancement of a photovoltaic thermal (PV/T) collector with periodically grooved channels. J Energy Storage 2021;40:102792. https://doi.org/10.1016/j.est.2021.102792.

[25] Zabihi Sheshpoli A, Jahanian O, Nikzadfar K, Aghajani Delavar M. Numerical and experimental investigation on the performance of hybrid PV/thermal systems in the north of Iran. Sol Energy 2021;215:108–20. https://doi.org/10.1016/j.solener.2020.12.036.

[26] Herrando M, Fantoni G, Cubero A, Simón-Allué R, Guedea I, Fueyo N. Numerical analysis of the fluid flow and heat transfer of a hybrid PV-thermal collector and performance assessment. Renew Energy 2023;209:122–32. https://doi.org/10.1016/j.renene.2023.03.125.

[27] Madadi M, Abbasian Arani AA. Experimental evaluation of photovoltaic thermal (PVT) system using a modular heat collector with flat back shape fins, pipe, nanofluids and phase change material. Sol Energy Mater Sol Cells 2025;280:113294. https://doi.org/10.1016/j.solmat.2024.113294.

[28] Poredoš P, Tomc U, Petelin N, Vidrih B, Flisar U, Kitanovski A. Numerical and experimental investigation of the energy and exergy performance of solar thermal, photovoltaic and photovoltaic-thermal modules based on roll-bond heat exchangers. Energy Convers Manag 2020;210:112674. https://doi.org/10.1016/j.enconman.2020.112674.

[29] Alqatamin A, Jinzhan S. Numerical analysis and design of photovoltaic-thermal (PVT) system with novel water-cooling channel structure integrated with perforated V-shape fins. Renew Energy 2025;243:122587. https://doi.org/10.1016/j.renene.2025.122587.

[30] Jabeen N, Waqas A, Ali M. Dynamic performance evaluation of PCM-based PVT systems: combined impact of design modifications and nanofluids. J Energy Storage 2025;121:116645. https://doi.org/10.1016/j.est.2025.116645.

[31] Zareie Z, Ahmadi R, Asadi M. A comprehensive numerical investigation of a branch-inspired channel in roll-bond type PVT system using design of experiments approach. Energy 2024;286:129452. https://doi.org/10.1016/j.energy.2023.129452.

[32] Maseer MM, Ismail FB, Kazem HA, Hachim DM, Al-Gburi KAH, Chaichan MT. Performance enhancement of photovoltaic/thermal collector semicircle absorber tubes using nanofluid and NPCM. Renew Energy 2024;233:121152. https://doi.org/10.1016/j.renene.2024.121152.

[33] Attia MEH, Zayed ME, Kabeel AE, Khelifa A, Arıcı M, Abdelgaied M. Design and performance optimization of a novel zigzag channeled solar photovoltaic thermal system: numerical investigation and parametric analysis. J Clean Prod 2024;434:140220. https://doi.org/10.1016/j.jclepro.2023.140220.

[34] Khelifa A, Kabeel AE, Attia MEH, Zayed ME, Abdelgaied M. Numerical analysis of the heat transfer and fluid flow of a novel water-based hybrid photovoltaic-thermal solar collector integrated with flax fibers as natural porous materials. Renew Energy 2023;217:119245. https://doi.org/10.1016/j.renene.2023.119245.

[35] Sopian K, Jin GL, Othman MY, Zaidi SH, Hafidz M. Advanced absorber design for Photovoltaic thermal (PV/T) collectors. Recent Res Energy Environ Landsc Archit 2011;978–1–6180:77–83.

[36] Météo El Jadida. meteoblue. https://www.meteoblue.com/fr/meteo/semaine/el-jadida_maroc_2550078. [Accessed 16 November 2025].

[37] Solar I-Ve | HT Instruments. https://www.ht-instruments.com/fr-fr/produits/testeurs-photovoltaique/controle-de-performance/solar-i-ve/. [Accessed 7 February 2026].

[38] Kline S, McClintock F. Describing uncertainties in single-sample experiments. Mech Eng 1963;75:3–8.
[39] Olmuş U, Güzelel YE, Çerçi KN, Büyükalaca O. Numerical analysis and comparison of different serpentine-based photovoltaic-thermal collectors. Renew Energy 2025; 241:122196. https://doi.org/10.1016/j.renene.2024.122196.
[40] Alami YE, Ouerradi F, Bounouar S, Benhmida M, Rhiat M, Benhala B, et al. Comparative study of the performance of photovoltaic and photovoltaic thermal solar systems: case study in El Jadida. E3S Web Conf 2025;601:00011. https://doi.org/10.1051/e3sconf/202560100011.
[41] El Alami Y, Baghaz E, Errebii M, Nasrin R, Amagour MEH, Al-Aribe KM, et al. Numerical perspective of copper nanoparticle morphology on energy conversion in a novel photovoltaic-thermal system. Energy 2026;342:139598. https://doi.org/10.1016/j.energy.2025.139598.
[42] El Alami Y, Baghaz E, Nasrin R, Chanaa F, Bendaoud R, Padmanaban S, et al. Experimental-numerical comparative study of performance and cost-effectiveness of partially- and fully-cooled photovoltaic thermal systems. Case Stud Therm Eng 2025;73:106660. https://doi.org/10.1016/j.csite.2025.106660.
[43] Rajamony RK, Pandey AK, Sofiah AGN, Wadaan MA, Siaw Paw JK, Suraparaju SK, et al. Energy, exergy, economic and environmental (4E) analysis of serpentine tube absorber photovoltaic thermal system using nano enhanced phase change material. Energy 2025;319:135032. https://doi.org/10.1016/j.energy.2025.135032.
[44] Azeez HL, Ibrahim A, Ahmed BO, Dol SS, Al-Waeli AHA, Jaber M. Experimental investigations of heat transfer, energy, and exergy-based sustainability of a novel photovoltaic thermal system. Case Stud Therm Eng 2025;70:106089. https://doi.org/10.1016/j.csite.2025.106089.
[45] Zohri M, Prabowo Suwarno, Solomin E, Yazdi MH, Suyono T, et al. Sustainability index and a bibliometric of photovoltaic thermal with rectangular channel. Case Stud Therm Eng 2024;63:105300. https://doi.org/10.1016/j.csite.2024.105300.
[46] Alami YE, Dahmani H, Ouerradi F, Zohal B, Bendaoud R, Baghaz E. Impact of heat exchanger materials on the performance of solar hybrid photovoltaic thermal (PVT) systems: 3D analysis. In: Hajji B, Gagliano A, Mellit A, Rabhi A, Calì M, editors. Proc. 4th int. Conf. Electron. Eng. Renew. Energy syst., vol. 2. Singapore: Springer Nature; 2025. p. 609–19. https://doi.org/10.1007/978-981-97-9975-6_58.
[47] Alami YE, Baghaz E, Nasrin R, Haboubi K, Benhmida M, Ibrahim A. Integrated sustainability and 4E analysis of hybrid nanofluid featured PVT systems incorporating diverse backsheets. Appl Therm Eng 2025:129147. https://doi.org/10.1016/j.applthermaleng.2025.129147.
[48] Nahar A, Hasanuzzaman M, Rahim NA. Numerical and experimental investigation on the performance of a photovoltaic thermal collector with parallel plate flow channel under different operating conditions in Malaysia. Sol Energy 2017;144: 517–28. https://doi.org/10.1016/j.solener.2017.01.041.
[49] Bisengimana E, Zhou J, Binama M, Yuan Y. Numerical investigation on the factors influencing the temperature distribution of photovoltaic/thermal (PVT) evaporator/condenser for heat pump systems. Renew Energy 2022;194:885–901. https://doi.org/10.1016/j.renene.2022.05.154.
[50] El Alami Y, Baghaz E, Bendaoud R, Nasrin R. Pressure drops reduction and performance optimization strategies of an innovative channel box Photovoltaic thermal system. Int J Photoenergy 2025;2025:8744508. https://doi.org/10.1155/ijph/8744508.
[51] Kazemian A, Salari A, Hakkaki-Fard A, Ma T. Numerical investigation and parametric analysis of a photovoltaic thermal system integrated with phase change material. Appl Energy 2019;238:734–46. https://doi.org/10.1016/j.apenergy.2019.01.103.
[52] Kazemian A, Salari A, Ma T. A year-round study of a photovoltaic thermal system integrated with phase change material in Shanghai using transient model. Energy Convers Manag 2020;210:112657. https://doi.org/10.1016/j.enconman.2020.112657.
[53] Ahmadinejad M, Soleimani A, Gerami A. The effects of a novel baffle-based collector on the performance of a photovoltaic/thermal system using SWCNT/Water nanofluid. Therm Sci Eng Prog 2022;34:101443. https://doi.org/10.1016/j.tsep.2022.101443.
[54] Kazemian A, Ma T, Hongxing Y. Evaluation of various collector configurations for a photovoltaic thermal system to achieve high performance, low cost, and lightweight. Appl Energy 2024;357:122422. https://doi.org/10.1016/j.apenergy.2023.122422.
[55] Karaaslan I, Menlik T. Numerical study of a photovoltaic thermal (PV/T) system using mono and hybrid nanofluid. Sol Energy 2021;224:1260–70. https://doi.org/10.1016/j.solener.2021.06.072.
[56] Zohri M, Ramadhan W, Fudholi A. Improvement potential and sustainability index of photovoltaic thermal solar air collector. Int J Heat Technol 2022;40:743–8. https://doi.org/10.18280/ijht.400312.
[57] Zohri M, Yuliadi Ghazali M, Idham. Performance of photovoltaic thermal technology using V-Absorber with exergy, improvement potential and sustainability index analysis. Math Model Eng Probl 2023;10:551. https://doi.org/10.18280/mmep.100223.
[58] Bestas S, Aktas IS, Bayrak F. A bibliometric and performance evaluation of nano-PCM-integrated photovoltaic panels: energy, exergy, environmental and sustainability perspectives. Renew Energy 2024;226:120383. https://doi.org/10.1016/j.renene.2024.120383.
[59] Atalay H, Tunçkal C, Türkdoğan S, Direk M. Exergetic, sustainability and exergoeconomic analyses of a fully photovoltaic-powered heat pump tumble dryer. Renew Energy 2024;225:120274. https://doi.org/10.1016/j.renene.2024.120274.
[60] Tirupati Rao V, Raja Sekhar Y, Arıcı M, Ralph Pochont N, Reddy Prasad DM. Experimental investigations on bi-symmetrical web flow water based photovoltaic-thermal (PVT) system: energy, exergy, and entropy (3-E) analysis. Sol Energy 2024; 271:112445. https://doi.org/10.1016/j.solener.2024.112445.
[61] Alktranee M, Al-Yasiri Q, Saeed Mohammed K, Al-Lami H, Bencs P. Energy and exergy assessment of a photovoltaic-thermal (PVT) system cooled by single and hybrid nanofluids. Energy Convers Manag X 2024;24:100769. https://doi.org/10.1016/j.ecmx.2024.100769.
[62] Kazemian A, Khosravi K, Sen S, Talebizadehsardari P, Cairns A, Ma T. Optimizing photovoltaic thermal systems with wavy collector tube: a response surface-based design study with desirability analysis. Appl Therm Eng 2025;258:124475. https://doi.org/10.1016/j.applthermaleng.2024.124475.
[63] Shahsavar A, Eisapour M, Talebizadehsardari P. Experimental evaluation of novel photovoltaic/thermal systems using serpentine cooling tubes with different cross-sections of circular, triangular and rectangular. Energy 2020;208:118409. https://doi.org/10.1016/j.energy.2020.118409.
[64] Mahdi ZM, Al-Shamani AN, Al-Manea A, Al-zurfi HA, Al-Rbaihat R, Sopian K, et al. Enhancing photovoltaic thermal (PVT) performance with hybrid solar collector using phase change material, porous media, and nanofluid. Sol Energy 2024;283: 112983. https://doi.org/10.1016/j.solener.2024.112983.
[65] Alous S, Kayfeci M, Uysal A. Experimental investigations of using MWCNTs and graphene nanoplatelets water-based nanofluids as coolants in PVT systems. Appl Therm Eng 2019;162:114265. https://doi.org/10.1016/j.applthermaleng.2019.114265.
[66] Maatallah T, Zachariah R, Al-Amri FG. Exergo-economic analysis of a serpentine flow type water based photovoltaic thermal system with phase change material (PVT-PCM/water). Sol Energy 2019;193:195–204. https://doi.org/10.1016/j.solener.2019.09.063.
[67] Mohtasim MdS, Paul UK, Kibria MdG, Das BK. 7E and sustainability analysis of photovoltaic thermal system (PVT) incorporating graphene and Al2O3 nano-particles with paraffin wax integrated fin arrangements. J Clean Prod 2025;519: 146007. https://doi.org/10.1016/j.jclepro.2025.146007.